Measurement Report: Enhanced contribution of photooxidation to dicarboxylic acids in urban aerosols during the COVID-19 lockdown in Jinan, East China

Jingjing Meng[1,2], Yachen Wang[1], Yuanyuan Li[1], Tonglin Huang[1], Zhifei Wang[3], Yiqiu, Wang[4], Min Chen[1], Zhanfang Hou[1], Kimitaka Kawamura[5], Pingqing Fu[2]

[1]School of Geography and Environment, Liaocheng University, Liaocheng 252000, China
[2]Institute of Surface-Earth System Science, School of Earth System Science, Tianjin University, Tianjin 300072, China
[3]Jinan Environmental Monitoring Center of Shandong Province, Jinan 250101, China
[4]Liaocheng Environmental Information and Monitoring Center, Liaocheng, 252000, China
[5]Chubu Institute for Advanced Studies, Chubu University, Kasugai 487-8501, Japan

Correspondence to: Pingqing Fu (fupingqing@tju.edu.cn)

Abstract. To curb the spread of a novel coronavirus pandemic (COVID-19), a preventive lockdown (LCD) policy was first implemented across China in early 2020, resulting in a substantial drop-off in anthropogenic pollutant emissions and thus the amelioration of air quality. Unexpectedly, several haze events driven by enhanced secondary organic aerosols (SOA) still took place in the eastern China during the LCD. To investigate the effect of LCD measures on the formation and evolutionary process of SOA, $PM_{2.5}$ samples were collected before and during the LCD in Jinan, East China. The samples were measured for dicarboxylic acids (diacids) and related compounds, water-soluble inorganic ions, carbonaceous species, as well as the stable carbon isotopic compositions ($\delta^{13}C$) of major diacids. Our results show that despite the sharp decrease of primary pollutants (e.g., CO, SO_2, NO_2, and element carbon) during the LCD, the O_3 concentration, proportion of secondary inorganic aerosols, concentration levels, and relative abundance of diacid homologues in water-soluble organic compounds (WSOC) were still 2−4 times higher than those before the LCD. The ratios of oxalic acid (C_2) to diacids (C_2/diacids) and to total detected organic components were higher during the LCD than those before the LCD, suggesting the more aged organic aerosols during the LCD under the clearer sky conditions. The temporal changes, diurnal variations in major diacids, and their higher concentrations and contributions during the LCD than before the LCD are mainly due to the enhanced photochemical oxidation by the higher O_3 and the stronger solar radiation during the LCD. Interestingly, compound-specific stable carbon isotope ratios ($\delta^{13}C$) of C_2 and other major diacids show higher values in the nighttime than the daytime before the LCD, which indicate a significant contribution of organic acids via aqueous phase oxidation at night. Source apportionments using the molecular characteristics of organic compounds and positive matrix factorization (PMF) model suggest that the aqueous oxidation (45.2%) and coal combustion (16.7%) were the major sources before the LCD but the photochemical oxidation promoted by the higher O_3 concentration (48.8%) and aqueous oxidation (17.7%) were the dominant source during the LCD. The increased $\delta^{13}C$ values of oxalic acid and other major organic acids along with the high ratios of C_2/Gly, C_2/mGly, and C_2/diacids before and during the LCD confirm an isotopic fractionation effect during the precursor oxidation processes. Furthermore, more positive $\delta^{13}C$ values of diacids are observed in the daytime than the nighttime during the LCD, which suggest an enhanced photochemical oxidation in the urban atmosphere during this period.

1 Introduction

Water-soluble organic compounds (WSOC), constituting a great proportion of atmospheric fine particles, have attracted a growing attention for the adverse effects on haze formation and global climate change (Lv et al., 2022; Wang et al., 2016). Dicarboxylic acids (diacids) and their organic precursors such as oxocarboxylic acids (oxoacids) and α-dicarbonyls are ubiquitous in the atmosphere, accounting for 14% of WSOC in urban regions (Ho et al., 2007; Kawamura and Bikkina, 2016), and can be up to 52% in marine area (Bikkina et al., 2015). Due to the high solubility and hygroscopic property, diacid homologues can not only modify the hygroscopic growth of aerosols, but also improve the cloud condensation nuclei (CCN) activation and ice nuclei (IN) formation, thus they exert an important effect on radiative forcing of aerosols via scattering the solar radiation and cloud formation (Ding et al., 2021; Wang et al., 2015).

Diacids and related compounds can be emitted directly from biogenic activity (Rinaldi et al., 2011), vehicle exhausts (Kawamura and Kaplan, 1987), and combustions of biomass and fossil fuels (Cao et al., 2017; Narukawa et al., 1999), while their relative contribution to total aerosol mass is negligible (Shen et al., 2022; Wang et al., 2020a). A growing body of evidence from model studies, chamber experiments, cloud observations, and field measurements have highlighted that most of these water-soluble organic aids are predominantly generated from the photochemical oxidation of volatile organic compounds (VOCs) followed by partitioning into the aqueous phase in wet aerosols, fog, and cloud droplets (Carlton et al., 2007; Ervens et al., 2004, 2011; Fu et al., 2008; Lim et al., 2013; Shen et al., 2022; Wang et al., 2010). Therefore, diacid homologues have been regarded as essential indicators of SOA in the atmosphere to trace the aging processes and assess the oxidative capacity of aerosols (Enami et al., 2015; Zhao et al., 2020). As the lowest molecular weight and the most abundant diacid, oxalic acid (C_2) has been proved to be mostly derived from two pathways: (1) photochemical breakdown (or decomposition) of longer-chain diacids (C_3–C_{11}) (Enami et al., 2015; Yu et al., 2021); and (2) secondary oxidation of VOCs via α-dicarbonyls including glyoxal (Gly) and methyglyoxal (mGly) in aqueous phase of aerosol and cloud droplets, which has been considered to dominate over the first pathway (Carlton et al., 2007; Xu et al., 2022).

More oxidized SOA are largely produced from aqueous oxidation, while less oxidized SOA are largely derived from gaseous photochemical oxidation (Hu et al., 2017; Yu et al., 2019). Yu et al. (2019) reported that aqueous oxidation exerts a dominant effect on diacids and related compounds despite the increased contribution of photochemical oxidation in gas phase during the haze events in Beijing using multiple linear regression. A recent study by Xu et al. (2022) pointed out that a large portion of C_2 was derived from the aqueous process of organic precursors emitted from fossil fuel combustion. Laboratory simulation has demonstrated that C_2 can be photodegraded under the O_3 chemical pathway (Gligorovski et al., 2010), but field measurements have demonstrated that O_3-dominated formation pathways are involved in the formation of C_2 (Meng et al., 2021; Mochizuki et al., 2017). The formation mechanism and influencing factors as well of the contribution of aqueous oxidation and gaseous photochemical oxidation are still not well understood. Therefore, further investigations on C_2 and related SOA are necessary to provide a knowledge base for improving air quality and the accuracy of model.

To curb the transmission of the novel coronavirus disease 2019 (COVID-19) in human society, a strict lockdown (LCD) measure was first implemented by the Chinese government starting at the end of January 2020 (Le et al., 2020). These dramatic restrictions resulted in a sharp drop-off of air pollutants (Li et al., 2021; Meng et al., 2021), for instance, the average concentrations of five parameters including CO, NO_2, SO_2, $PM_{2.5}$, and PM_{10} decreased by 4.6–24.7% in 44 cities of China because of the travel restrictions during the LCD (Bao and Zhang, 2020). Unexpectedly, a few haze episodes still occurred in China during the LCD. Online observations, model simulations, and satellite measurements have pointed out that the appearance of haze events during the LCD were mainly caused by the unfavorable meteorological conditions, continuous emissions of SO_2, NO_X and VOCs from power plants and petrochemical refineries, and an enhanced SOA formation (Huang et al., 2020; Li et al., 2020; Wang et al., 2020b; Shi et al., 2021; Zhong et al., 2021). These studies focused on the effect of the LCD policies on air quality and haze formation, for example, Le et al. (2020) and Huang et al. (2020) pointed out that the reduction of NO_X emissions lead to the enhanced ozone concentration, further improved the atmospheric oxidizing capacity

and promoted the formation of secondary aerosol during the LCD. However, little is known about the impact of LCD measures on the molecular distributions, aging processes, and the formation mechanisms of SOA from field observations.

In order to understand the effect of the reduced anthropogenic emissions during the LCD and different meteorological parameters on the evolutionary process of homologous diacids and to investigate the relative contribution of aqueous oxidation versus photochemical oxidation to total diacid homologues, we collected fine aerosol samples in urban Jinan, East China on a day/night basis before and during the LCD. We compare the differences in the molecular distributions, stable carbon isotopic compositions, and formation processes of C_2 and the related SOA before and during the LCD. Then, we investigate the effect of meteorological parameter (e.g., RH, temperature, and solar radiation) and aerosol aqueous properties (e.g., liquid water content (LWC) of aerosol and particle acidity (pH_{is})) on their formation processes in the urban atmosphere.

2 Experimental methods

2.1 Aerosol sampling

Fine aerosol ($PM_{2.5}$) sampling was conducted on the rooftop of a six-story building (36.67 °N, 117.06 °E, approximately 20 m above ground) that was about 40 m away from the Jinan Environment Monitoring Center (one of the State Controlling Air Sampling Sites in Jinan). The sampling site is in the center of Jinan city, which is located in the midwestern part of Shandong Province, China (Fig. S1). The sampling site lies in a typical urban setting surrounded by heavy traffic roads, residential areas, and commercial centers. $PM_{2.5}$ samples were collected using prebaked (450 °C, 8 h) quartz fiber filters (8 in. × 10 in.) from 6 January to 17 February 2020. The government of Shandong Province first performed the preventive LCD starting on 24 January 2020; thus the whole sampling period was divided into two periods: (1) before the LCD from 6 to 23 January, (2) during the LCD from 31 January to 17 February. Each sample lasted for 12 h on a day/night basis using a high-volume air sampler (TISCH, USA) at an airflow rate of 1.013 m^3 min^{-1}. The daytime samples were collected from 8:00 to 20:00, while nighttime samples were collected from 20:00 to 8:00 of the next day. Field blank samples were also collected by mounting the blank filter onto the sampler for 10 min without turning on the sampler before, during, and after the sampling campaign, respectively. A total of 72 $PM_{2.5}$ samples (36 for daytime and 36 for nighttime) and 6 field blank samples were collected in the whole sampling period. After the collection, each filter was sealed in an aluminum foil bag and stored in a freezer (−20 °C) for about 16 months prior to analysis. The concentrations of $PM_{2.5}$, PM_{10}, CO, SO_2, NO_2, and O_3 as well as meteorological parameters such as wind direction/speed, RH, temperature, and solar radiation were retrieved from the monitoring station in the Jinan Environment Monitoring Center (https://www.aqistudy.cn/). The detail information of quality assurance/quality control (QA/QC) of online data was described in Text S4. The inlet height of the air quality monitoring station was approximately 20 m above the ground level.

2.2 Chemical Analysis

2.2.1 Determination of diacids and related compounds as well as levoglucosan

The quantitative method for analyzing diacids, oxoacids, and α-dicarbonyls in $PM_{2.5}$ has been described previously (Fu et al., 2013; Meng et al., 2020). Briefly, a quarter of the filter was extracted with 5 mL pure Milli-Q water under ultrasonication for three times. The water extracts were concentrated to near dryness and then reacted with 14% BF_3/n-butanol at 100 °C for 1 hour. During this process, the carboxyl functional group was derivatized to butyl ester, and the aldehyde and keto groups were derived to dibutoxy acetal. After derivatization, n-hexane was added and washed with pure water for three times. Finally, the hexane layer was determined by a gas chromatography-mass spectrometry (GC-MS) and quantificationally analyzed using a GC (Agilent 6980) coupled with an HP-5 column (0.2mm × 25m, 0.5 μm film thickness) and a flame

ionization detector (FID). GC-MS was performed on a Hewlett-Packard model Agilent 7890A GC coupled to a Hewlett-Packard model Agilent 5975C mass selective detector (MSD). GC separation was equipped with a split/splitless injector and a fused silica capillary column (DB-5MS, 30 m × 0.25 mm i.d., 0.25 μm film thickness). The GC oven temperature was programmed from 50°C for 2 min to 120°C at a rate of 15°C min^{-1}, and then to 300°C at a rate of 5°C min^{-1} with a final hold at 300°C for 16 min. The mass spectrometer was operated on the electron impact (IE) mode at 70 eV and scanned from 50 to 650 Da. The same analytical method as described above was also applied for field blank filters. Recoveries of the target compounds were 80% for C_2 and higher than 85% for other organic species.

Additionally, another portion of each filter sample was extracted with a mixture of dichloromethane and methanol (2:1, *v/v*) under ultrasonication. After being derivatized with 60 μL mixture of N, O-bis-(trimethylsilyl) trifluoroacetamide (BSTFA) and pyridine (5:1, *v/v*) at 70°C for 3 h, and the derivatized extracts were identified for levoglucosan using a GC-MS (Yi et al., 2021). The recovery rate of levoglucosan is higher than 95%. Compared with the ambient samples, the concentration of levoglucosan in the field blank samples was lower than 4%. The data of targeted organic species presented in this study were corrected for both recoveries and field blanks.

2.2.2 Stable carbon isotopic composition of diacids and related compounds

The stable carbon isotopic compositions (δ^{13}C) of major diacids and related compounds were measured using the method reported elsewhere (Kawamura and Watanabe, 2004). Briefly, 2 μL internal standard (*n*-C_{13} alkane, -27.24 ‰) was spiked to the ester fraction, the δ^{13}C values of the derivatized samples relative to Pee Dee Belemnite (PDB) were identified using a GC-isotope ratio MS (GC-IR-MS, Thermo Fisher, Delta V Advantage). GC was installed with a HP manual on-column injector and a capillary column (CIP-Sil 8CB, 60 m × 0.32 mm × 0.25 μm) was used with a column oven temperature programmed from 50 to 120°C at a rate of 30°C min^{-1} and then to 300°C at a rate of 6°C min^{-1}. Flow rate of carrier gas (He) was maintained at 1.7 mL min^{-1}. Each sample was measured twice or three times to check the analytical error of the δ^{13}C values, which were less than 0.2‰. The δ^{13}C values were then calculated for free organic acids using an isotope mass balance equation based on the measured δ^{13}C values of derivatives and the derivatizing agent (BF$_3$/*n*-butanol), as detailed in Text S1 (Kawamura and Watanabe, 2004).

2.2.3 Elemental carbon (EC), organic carbon (OC), WSOC, and inorganic ions

EC and OC in the PM$_{2.5}$ samples were analyzed using a DRI Model 2015 Carbon Analyzer following the Interagency Monitoring of Protected Visual Environments (IMPROVE) thermal/optical reflectance (TOR) protocol (Chow et al., 2004). As for the measurement of inorganic ions and WSOC, an aliquot of each sample filter was extracted with 30 mL Milli-Q water using an ultrasonic bath for three times, and then filtered through PTFE filters to remove particles and filter debris. The water extract was then divided into two parts. One part was analyzed for inorganic ions using an ion chromatography (Dionex 600, USA), and the other part was used to determine WSOC using a Total Carbon Analyzer (TOC-L CPH, Shimadzu, Japan).

2.3 Calculation of aerosol liquid water content (LWC) and particle in-situ pH (pH$_{is}$)

As for the calculation of aerosol LWC and pH$_{is}$, the ISORROPIA-II model that treated the Na$^+$ - NH$_4^+$ - K$^+$ - Ca^{2+} - Mg^{2+} - SO$_4^{2-}$ - NO$_3^-$ - Cl$^-$ system was applied. The forward mode with a metastable state in the ISORROPIA model was adopted (Fountoukis and Nenes, 2007).

3 Results and Discussion

3.1 Overview of observations

Temporal variations in the concentrations of $PM_{2.5}$, PM_{10}, gaseous pollutants,major chemical components of $PM_{2.5}$, and meteorological parameters before and during the LCD are summarized in Table 1 and presented in Fig. 1. Both temperature and solar radiation exhibited a continuously increasing trend, whereas RH before the LCD was 1.4 times higher than that during the LCD. Wind speed (3.0 ± 0.7 m s^{-1}) before the LCD was smaller than that (3.7 ± 1.1 m s^{-1}) during the LCD (Table 1), suggesting that air pollution caused by emissions from the local and surrounding regions of Jinan city before the LCD was greater than that during the LCD, which was supported by the results of backward trajectory and PSCF analysis (Fig. S1)

The parameters of air quality including $PM_{2.5}$, PM_{10}, CO, SO_2, and NO_2 reduced by 39.3–62.4% during the LCD (Table 1, Fig. 1), suggesting that the air quality was better during the LCD because of the substantial reduction of anthropogenic emissions. O_3 in Chinese megacities during the wintertime is primarily produced from the NOx-saturated regime because of the lack of HOx radicals (Li et al., 2021). Being opposite to other five air-quality parameters, O_3 concentration (66.3 ± 21.0 μg m^{-3}) during the LCD increased by 2.3 times compared to that (28.9 ± 18.2 μg m^{-3}) before the LCD (Table 1), which would facilitate the SOA formation through O_3-dominated photochemical oxidation. The more favorable meteorological conditions including the higher temperature and the stronger solor radiation (Meng et al., 2021), and the remarkable decrease in $PM_{2.5}$ concentraion during the LCD could facilitate more O_3 formation (Wu et al., 2020). Moreover, the significant reduction of NO_2 during the LCD could lead to the substaintial drop of NO, and ultimately weakened the chemical loss of O_3 through NO titration (NO + O_3 = NO_2 + O_2) (Wang et al., 2022). A recent study using the WRF−Chem model found that about 80% of the increased O_3 level in eastern China was mainly due to meteorological changes, and only 20% resulted from the reduced pollutant emissions (Wang et al., 2022).

The decreased concentrations of EC, OC, and WSOC in $PM_{2.5}$ but the enhanced ratios of OC/EC and WSOC/OC during the LCD (Table 1, Fig. 1) indicated more SOA productions due to the stronger photochemical oxidation during the LCD (Zhong et al., 2021). As a key tracer for biomass burning, levoglucosan showed a positive relationship with OC, EC, and WSOC ($R^2 \geq 0.45$) before the LCD rather than during the LCD ($R^2 \leq 0.15$) (Table S1), suggesting that biomass burning played an important role on carbonaceous species before the LCD rather than during the LCD. Secondary inorganic ions (SIA, total concentration of SO_4^{2-}, NO_3^-, and NH_4^+) were dominant components of $PM_{2.5}$, which accounted for the higher percentages ($46.9 \pm 8.2\%$) in $PM_{2.5}$ mass during the LCD than that ($39.9 \pm 6.5\%$) before the LCD, indicating an enhanced formation of secondary aerosols during the LCD. The LWC concentration of aerosol is determined by RH and SIA concentration (Meng et al., 2020). In view of the higher RH and SIA concentration before the LCD, the LWC concentration (34.8 ± 32.7 μg m^{-3}) before the LCD was 3.4 times higher than that (10.1 ± 10.0 μg m^{-3}) during the LCD. However, pH_{is} remained similar before (3.2 ± 3.0) and during the LCD (3.5 ± 3.1) with no significant statistical difference ($p > 0.05$, Table S2), indicating an insignificant difference in atmospheric aerosol acidity before and during the LCD.

3.2 Molecular distributions of diacids and related species

A homogeneous series of diacids (C_2–C_{11}), oxoacids, and α-dicarbonyls identified in $PM_{2.5}$ samples before and during the LCD are summarized in Table 2. To avoid the effect of atmospheric dilution due to the boundary layer height variations, here we use the ratios of SOA species to EC or CO to explore the secondary production of organic species (Yu et al., 2021). As shown in Fig. 2, the ratio of total concentration of detected organic components (TDOCs) normalized by CO (TDOCs/CO) increased exponentially with the enhancement of temperature before and during the LCD ($R^2 > 0.5$), which agreed well with the Arrhenius Law, confirming that TDCOCs in this study were primarily derived from secondary formation and the contribution of primary emissions was negligible. Additionally, the exponent number (0.067) of the

regression trend line during the LCD was 3.5 times higher ($p < 0.05$) than that (0.019) before the LCD, indicating that the oxidation rate during the LCD was larger, largely due to the more favorable meteorological conditions. To verify if the concentrations of target compounds and major ratios were of significant difference, statistic test was performed for $PM_{2.5}$ samples before and during the LCD (Table S2 and Table S3). As shown in Table S2, the concentrations of organic species (except for α-dicarbonyls) and major ratios in $PM_{2.5}$ before and during the LCD presented p values less than 0.05, indicating that the abundances and compositions of the major species before and during the LCD were statistically different. TDOCs exhibited an upward trend from 437 ±117 μg m^{-3} (246 – 833 μg m^{-3}) before the LCD to 486 ±144 μg m^{-3} (179 –825 μg m^{-3}) during the LCD (Table 2). The concentrations of diacids and oxoacids during the LCD increased by 1.1 and 2.1 times, respectively, while α-dicarbonyls during the LCD was almost the same to that before the LCD.

The daytime concentration of diacids before the LCD was 17% lower than that at night, which was opposite to the diurnal variation of diacids concentration during the LCD (Fig. 3a). As the predominant species throughout the whole observation period, C_2 concentration increased from 181 ±47.5 m^{-3} before the LCD to 239 ± 108 μg m^{-3} during the LCD (Table 2), despite of the significant decrease in the primary pollutants from anthropogenic emissions during the LCD. C_2 is an end product derived from photochemical decomposition of longer-chain diacids or secondary oxidation of α-dicarbonyls and oxoacids, thus the ratios of C_2/diacids and C_2/TDOCs can be considered essential tracers for aerosol aging (Wang et al., 2012; Zhao et al., 2020). Both ratios of C_2/diacids and C_2/TDOCs during the LCD were higher than those before the LCD (Fig. 3b), reflecting the more aged organic aerosols during the LCD. Therefore, the concentration of C_2 as well as its relative abundance in total diacids and TDOCs were higher during the LCD than those before the LCD, mainly due to the accelerated formation of C_2 during the LCD, which could offset the drop of organic precursors from anthropogenic emissions (Huang et al., 2020). Moreover, the daytime concentration of C_2 and the ratios of C_2/TDOCs and C_2/diacids were lower than those at night before the LCD but an opposite trends were found during the LCD, being consistent with the diurnal changes of total diacids before and during the LCD (Fig. 3b). The second most abundant diacid was succinic acid (C_4), followed by malonic acid (C_3) and azelaic acid (C_9) before the LCD, while the second dominant diacid during the LCD was C_3, followed by C_4 and phthalic acid (Ph) (Table 2). These results suggested that these species had different sources and underwent different formation processes before and during the LCD. Both ratios of C_2/C_4 and C_3/C_4 have been used as indicators of photochemical aging of diacids, because the hydroxylation of C_4 can be photodegraded into C_3 through the decarboxylation process, and C_3 can be photochemically oxidized into C_2 via intermediates (e.g., ketomalonic (kC_3) and hydroxymalonic acids) (Kawamura and Bikkina, 2016; Wang et al., 2010). Both C_2/C_4 (8.4 ±3.4) and C_3/C_4 (1.6 ±0.4) ratios during the LCD were higher than those (3.9 ±1.5, 0.3 ±0.1) before the LCD (Fig. 3b), indicating the stronger photochemical transformation of organic aerosols from the local oxidation and long-range transport during the LCD.

Azelaic acid (C_9) is primarily derived from the secondary oxidation of unsaturated fatty acids (e.g., oleic acid) with a double bond at the C-9 position (Kawamura and Usukura, 1993), which is abundant in the fresh and aged aerosols emitted from biomass burning (Shen et al., 2022). It is noteworthy that C_9 concentration (12.0 ±4.0) before the LCD was 2.0 times higher than that (5.9 ±4.8) during the LCD (Table 2), which was consistent with the variation of levoglucosan concentration (Table 1). C_9 showed a more robust relationship with levoglucosan before the LCD ($R^2 = 0.74$) than that ($R^2 = 0.06$) during the LCD (Table S1), suggesting that biomass burning was an essential contributor to C_9 before the LCD rather than during the LCD. Ph is primarily derived from the photochemical degradation of aromatic hydrocarbons (e.g., naphthalene) emitted from anthropogenic sources (Kawamura and Usukura, 1993). Although Ph was the most abundant diacid except for $C_2 – C_4$ during the LCD, its concentration (8.8 ± 6.1 μg m^{-3}) and relative abundance (2.3 ±2.2%) during the LCD were lower than those (11.0 ± 6.1 μg m^{-3}, 3.2 ± 1.5%) before the LCD (Table 2, Fig. 3b), suggesting the remarkable drop of anthropogenic emissions during the LCD.

As the important intermediate compounds of mono-carboxylic acids, oxoacids can ultimately generate diacids through heterogeneous oxidation processes (Wang et al., 2012; Yu et al., 2021). The diurnal variations of oxoacids presented similar

patterns with diacids in each period (Fig. 3a). Moreover, oxoacids correlated well with total diacids in each period, respectively ($R^2 > 0.5$, Fig. 2), indicating that oxoacids are the important intermediate species of diacids. The molecular distributions of oxoacids were characterized by the predominance of glyoxylic acid (ωC_2) and pyruvic acid (Pyr) in each period. Previous studies have demonstrated that C_2 in urban aerosols is mainly generated from ωC_2 via aqueous oxidation (Cheng et al., 2015; Zhao et al., 2018). Therefore, C_2 positively correlated with ωC_2 and SO_4^{2-} before and during the LCD, respectively ($R^2 > 0.5$, Fig. S2).

As the two smallest molecular weight α-dicarbonyls in the aerosols, glyoxal (Gly) and methylglyoxal (mGly) are originated from the photochemical oxidation of volatile organic compounds such as aromatics, isoprene, and monoterpenes in the gaseous phase, which are then partitioned into the aqueous phase of aerosols, and ultimately are oxidized to relatively lower volatility organic acids (e.g., ωC_2, Pyr, and C_2) (Carlton et al., 2007; Fu et al., 2008). Although the anthropogenic source emissions of α-dicarbonyls decreased dramatically during the LCD, the higher temperature and O$_3$ concentration during the LCD provided a favorable condition for α-dicarbonyls productions via secondary oxidation, which could offset the drop of primary emissions. Therefore, the concentration (24.7 $\pm$ 10.0 $\mu g\ m^{-3}$) of α-dicarbonyls during the LCD was about equal to that (25.1 $\pm$ 13.5 $\mu g\ m^{-3}$) before the LCD.

3.3 Aqueous formation of SOA before the LCD

The nighttime concentrations of C_2, diacids, and TDOCs exhibited higher values than those during the daytime as discussed above. Such diurnal variations may be ascribed to the descended planetary boundary layer (PBL) height at night, which can cause the enhanced concentrations of C_2 and related SOA. However, the increase in the ratios of C_2/diacids and C_2/TDOCs at night indicated that the effect of lowered nighttime PBL height was minor, which could be supported by the insignificant diurnal differences of primary pollutant markers such as Na^+, Ca^{2+}, and Mg^{2+} ($p > 0.05$, Table S3) between the daytime and nighttime. Considering the higher RH and LWC concentration at night, the increased concentrations of C_2 and related SOA during the nighttime may be closely linked to the accelerated aqueous production (Cheng et al., 2015; Meng et al., 2020).

The molecular pattern of TDOCs was predominated by C_2 followed by C_4 and C_3 as discussed above, consistent with the molecular distribution in biomass burning smoke (Kawamura et al., 2013; Kundu et al., 2010; Meng et al., 2020; Sorathia et al., 2018). To explore the contribution of biomass burning to TDOCs, levoglucosan and K^+ were proposed as reliable makers for biomass burning (Hoffmann et al., 2010; Huang et al., 2006). K^+ is abundant in aerosols emitted from biomass burning (Andreae, 1983), thus K^+ exhibited a close correlation with levoglucosan ($R^2=0.77$, Table S1) before the LCD. There was no obvious diurnal difference of levoglucosan and K^+ between daytime (140 $\pm$ 54.9 ng m^{-3}, 2.0 $\pm$ 0.1 $\mu g\ m^{-3}$) and nighttime (141 $\pm$ 84.4 ng m^{-3}, 2.1 $\pm$ 0.4 $\mu g\ m^{-3}$), suggesting that the higher concentrations of C_2 and related SOA at night were irrelevant to the difference in the emission strength of organic precursors from biomass burning in the daytime and nighttime. C_2, diacids, and TDOCs exhibited strong correlations with levoglucosan and K^+ before the LCD ($R^2 > 0.5$), while such correlations were not observed during the LCD ($R^2 < 0.2$) (Table S1), suggesting that biomass burning was an essential contributor to C_2 and related SOA before the LCD rather than during the LCD. The ratio of C_2/levoglucosan (1.7 $\pm$ 0.6) at night before the LCD exhibited larger value than that (1.3 $\pm$ 0.5) in the day, which was mainly ascribed to the accelerated aqueous formation of C_2 at night. Moreover, the mean values of C_2/levoglucosan (1.5 $\pm$ 0.6), C_2/K^+ (0.2 $\pm$ 0.03), C_4/levoglucosan (0.4 $\pm$ 0.1), and C_4/K^+ (0.05 $\pm$ 0.02) ratios before the LCD were higher than those (0.05, 0.05, 0.03, 0.03) in fresh particles emitted from savanna fires of southern African (Gao et al., 2003). It is interesting to note that the average ratios of C_2/C_4 (3.9 $\pm$ 1.5), C_3/C_4 (0.3 $\pm$ 0.1), and C_2/diacids (0.52 $\pm$ 0.55) before the LCD were almost equal to those (3.8, 0.3, and 0.55) measured in the aerosols for two days aging biomass samples via chamber experiment (Shen et al., 2022), suggesting that C_2 and related SOA before the LCD were linked tightly to the secondary oxidation of organic precursors emitted from biomass burning.

To explore the formation pathways and contributing factors of C_2 and related SOA before the LCD, the temporal variations of major diacids, LWC, pH$_{is}$, and meteorological parameters (e.g., solar radiation, temperature, and RH) were illustrated in

Fig. 4. The SO_4^{2-} formation was largely from aqueous phase oxidation (Sun et al., 2013; Zhang et al., 2015), thus the correlation analysis between SO_4^{2-} and C_2 can used to evaluate the formation process of C_2 mainly via aqueous phase pathways (Sorathia et al., 2018). C_2 was correlated significantly with SO_4^{2-} in the daytime ($R^2 = 0.53$) and nighttime ($R^2 = 0.66$) (Fig. S2) before the LCD, confirming the dominant aqueous-phase formation pathway of C_2. It is worth noting that the slope of the regression line of C_2/SO_4^{2-} ratio (0.005) at night was 1.3 times higher than that (0.004) during the daytime (Fig. S2b). Both the higher slop and C_2 concentrations indicate a more efficient formation of C_2 at night, largely because the C_2 production requires multiple steps of aqueous oxidation from VOCs while the formation of SO_4^{2-} requires fewer steps (Miyazaki et al., 2009). Noticeably, the concentrations of C_2 and diacids, as well as $C_2/diacids$ ratio culminated on the nighttime of January 23, which was characterized by significantly higher LWC concentration (172 µg m^{-3}) and RH (86.9%) (Fig. 4). The conditions of higher LWC and RH are favorable for the partitioning of Gly and mGly from gaseous phase to aqueous phase (Carlton et al., 2006; Meng et al., 2021). Thus, C_2 and its precursors (e.g., Gly and mGly) were positively correlated with RH and LWC, respectively ($R^2 > 0.45$, Fig. 5). Moreover, the ratios of C_2/Gly and $C_2/mGly$ also showed a significant correlation with RH and LWC ($R^2 > 0.4$, Fig. 5). Such strong correlations suggest that the higher LWC concentration and RH could not only promote the formations of C_2 and its precursors, but also facilitate the transformation of C_2 from the organic precursors.Therefore, LWC and RH can be regarded as vitally important factors controlling the aqueous production of C_2. The nighttime concentration of LWC and RH were higher than those during the daytime, which led to the higher concentration and percentage contribution of C_2 in the nighttime.

Previous studies have reported that C_2 can also be derived from the chain-breaking of longer-chain diacids in the aqueous phase (Kawamura and Usukura, 1993; Miyazaki et al., 2009). However, there was moderate or no serious correlation between C_2 and longer-chain diacids (e.g., C_3 and C_4), respectively ($R^2 < 0.3$, Fig. 5). Furthermore, longer-chain diacids and the ratios of C_2/C_3 and C_2/C_4 exhibited no significant correlation with LWC or RH ($R^2 < 0.24$, Fig. 5). It can be concluded the effect of chain-breaking of longer homologous diacids on aqueous formation mechanism of C_2 was negligible in this study. Numerous studies have reported that the acidic condition of aerosol is beneficial to the BSOA formation such as 2-methylglyceric acid from BVOCs (e.g., isoprene), and ultimately be transformed into C_2 via Gly, mGly, and ωC_2 in the aqueous phase by acid-catalyzed oxidation reactions (Surratt et al., 2007). Laboratory experiment has pointed out that the acidic environment of aerosol can accelerate the uptake and production of Gly and mGly via acidic-catalyzed heterogeneous oxidation (Jang et al., 2002). Therefore, pH_{is} exhibited pronounced negative relationships with C_2 and its precursors such as Gly and mGly ($R^2 \geq 0.45$, Fig. 5). Therefore, we could conclude that C_2 before the LCD was dominantly derived from the acidic-catalyzed aqueous oxidation with α-dicarbonyls rather than longer-chain diacids determined by RH and LWC.

3.4 Enhanced O_3-dominated formation of SOA during the LCD

As discussed in Section 3.2, the concentrations of C_2, diacids, and TDOCs as well as the ratio of $C_2/diacids$ during the LCD were higher than those before the LCD, despite the anthropogenic source strength dropped dramatically during the LCD. Given the higher O_3 concentration and stronger solar radiation during the LCD (Table 1), it can be expected that the enhanced concentration and contribution of C_2 were driven by the promoted photochemical oxidation, which was supported by the significantly higher C_3/C_4 ratio (1.6 ± 0.4) during the LCD than that (0.3 ± 0.1) before the LCD. Since C_3 can be generated from photochemical oxidation of C_4 in the atmosphere (Kawamura and Bikkina, 2016), the relatively high C_3/C_4 ratio during the LCD (Fig. 3b) indicates that aerosols during the LCD experienced more substantial photochemical aging. Field measurements and chamber experiments have reported that C_2 can be principally originated from photochemical oxidation of α-dicarbonyls from VOCs driven by O_3 and OH·radicals (Meng et al., 2021; Mochizuki et al., 2017). Bikkina et al. (2021) reported a laboratory production of oxalic and other LMW diacids together with intermediate oxoacids and α-dicarbonyls by ozonolysis of isoprene. O_3 was considered as a major marker for oxidant concentration of photochemical oxidation because OH·radical was unavailable in this study. In addition, solar radiation could also be used as a reliable

proxy for photochemical productions of C_2 and other diacids (Deshmukh et al., 2018). In view of the significant escalation of O_3 concentration and solar radiation during the LCD, it could be concluded that the productions of C_2 and related compounds may be closely involved in the O_3-dominated photochemical pathways under the stronger solar radiation.

To investigate the formation mechanism and potential sources of C_2 and related SOA during the LCD, the temporal variations in C_2 and its precursors, O_3, as well as meteorological factors are presented in Fig. 4. It is interesting to note that the highest O_3 concentration was observed on the daytime of January 31 when the concentrations of C_2 and diacids reached their peaks. Moreover, both C_2 and diacids concentrations as well as the C_2/diacids ratio exhibited robust correlations with O_3 ($R^2 > 0.5$, Fig. 6), respectively, suggesting that O_3 played an important role in the formation of C_2 and other diacids. Additionally, C_2 and diacids concentrations exhibited similar patterns of variations (Fig. 4) and strong correlations ($R^2 > 0.5$, Fig. 6) with solar radiation during the daytime. However, such similarities and strong correlations of those were not observed with temperature ($R^2 < 0.2$, Fig. 4 and Fig. 6), suggesting that the effect of temperature on the photochemical formation of C_2 was negligible. The enhancement of temperature can promote the productions of C_2 and its precursors (Meng et al., 2018), while the increase in the temperature can accelerate the volatilization of C_2, leading to the drop of C_2 concentration in the aerosol phase (Bilde et al., 2015). These results confirmed that C_2 and other diacids were overwhelmingly derived from the O_3-dominated photochemical processes driven by the stronger solar radiation.

Numerous studies have demonstrated that the longer-chain diacids can be photochemically degraded into C_2 (Kawamura and Bikkina, 2016; Zhao et al., 2020). It is worth noting that C_2 was correlated strongly with longer-chain diacids such as C_3 and C_4, respectively ($R^2 > 0.5$, Fig. 6). The ratio of C_2/diacids was correlated strongly with the ratios of C_3/C_4 ($R^2 = 0.68$) and C_2/C_4 ($R^2 = 0.58$, Fig. 6), indicating that C_2 may be largely derived from the photochemical degradation of higher molecular weight homologues of diacids. However, the correlation of the C_2/diacids ratio with $(C_3–C_{11})$-C/WSOC ($R^2 = 0.12$) was weak, primarily because the supply rates of longer-chain diacids have been demonstrated to be faster than their degradation rates of forming C_2 (Zhao et al., 2020). C_2/diacids was correlated robustly with solar radiation during the daytime ($R^2 = 0.76$, Fig. 6). Previous study suggested that the correlation analysis of C_2/diacids, C_2/C_4, and C_3/C_4 with O_3 could indicate the photochemical chain-breaking of longer-chain diacids producing C_2 (Liu et al., 2021). These ratios were observed to be correlated significantly with O_3 ($R^2 > 0.45$, Fig. 6). These results confirm that C_2 during the LCD was primarily originated from the photochemical degradation of longer-chain homologous diacids that was driven by stronger solar radiation and higher O_3 concentration rather than higher temperature.

The photochemical oxidation of Gly and mGly has been proposed as a considerable regional and global source of C_2 (Carlton et al., 2007; Fu et al., 2008). Gly can be firstly oxidize to ωC_2 and subsequently to C_2, while mGly can be oxidized to C_2 via Pyr (Wang et al., 2012; Warneck, 2003). The correlations of C_2 with Gly ($R^2 = 0.51$) and ωC_2 ($R^2 = 0.53$) were stronger than those with mGly ($R^2 = 0.38$) and Pyr ($R^2 = 0.04$) (Fig. 6). Carlton et al. (2007) have reported that the oxidation rate of Gly (3×10^{10} M^{-1} s^{-1}) with OH $\cdot$ radicals is faster than that of mGly (1.1×10^9 M^{-1} s^{-1}). Moreover, the C_2/Gly ratio was correlated significantly with O_3 ($R^2 = 0.49$, Fig. 6), whereas C_2/mGly ratio exhibited no correlation with O_3 ($R^2 = 0.03$, Fig. 6). These results suggest that the photochemical oxidation of Gly via ωC_2 contributed more to the formation of C_2 than the oxidation of mGly via Pyr, in which O_3 was an important influencing factor.

3.5 Stable carbon isotopic compositions of diacids

3.5.1 Differences in $\delta^{13}C$ values before and during the LCD

$\delta^{13}C$ of specific organic acids can provide insights into the photochemical aging (or processing) of organic aerosols due to isotopic fractionation of carbon during the phase partitioning and/or photochemical oxidation (Wang et al., 2020a; Zhang et al., 2016). On average, most of the detected diacid homologues exhibited higher $\delta^{13}C$ values during the LCD than those before the LCD (Table 3, Fig. 7). A previous study demonstrated that the enhanced $\delta^{13}C$ values in diacid homologues were found with UV irradiation time (Pavuluri and Kawamura, 2016). Additionally, Shen et al. (2022) reported that the $\delta^{13}C$ value

for C_2 in the 7-d aged biomass samples was higher than in the 2-d aged biomass samples using the combustion chamber. Thus, the enrichment of $\delta^{13}C$ values in diacid homologues during the LCD was mainly due to the promoted photochemical oxidation driven by the higher O_3 and the stronger solar radiation during the LCD. Similar to the diurnal variations in major diacids' concentrations, the nighttime $\delta^{13}C$ values of these detected diacids were more positive (or more negative) than those in the daytime before (or during) the LCD, which was ascribed to their different sources and formation processes in these two observation periods. In brief, the $\delta^{13}C$ values exhibited a decreasing trend as the carbon numbers of diacids increased (Fig. 7), consistent with other observation campaigns elsewhere (Meng et al., 2020; Pavuluri and Kawamura, 2016; Wang and Kawamura, 2006). The mean $\delta^{13}C$ value ($-20.3 \pm 2.5‰$) of C_2 was the heaviest in each period (Table 3), which was comparable to that ($-19.8 \pm 3.5‰$) observed in its surrounding city such as Liaocheng (Meng et al., 2020), and higher than the values obtained in other China's megacities such as Beijing ($-22.9 \pm 3.4‰$) (Zhao et al., 2018) and Xi'an ($PM_{2.1}$: from -21.1 to -23.5 ‰) (Wang et al., 2012), but smaller than the values measured in the Korea Climate Observatory at Gosan ($-15.8 \pm 4.3‰$) of East Asia (Zhang et al., 2016) and western Pacific and Southern Ocean ($-16.8 \pm 0.8‰$) (Wang and Kawamura, 2006) in the winter (Fig. 8). It is worth noting that the average $\delta^{13}C$ value of C_2 ($-22 \pm 1.9‰$) before the LCD was equal to that ($-21.9 \pm 1.2‰$) determined in the 2 d biomass samples (Shen et al., 2022) (Fig. 8), confirming that biomass burning and subsequent oxidation exerted an important effect on C_2 before the LCD.

As mentioned above, C_2 can be not only originated from the photochemical breakdown (or decomposition) of C_3 and C_4 via kC_3 and hydroxymalonic acids (hC_4), but also be derived from the photochemical oxidation of aromatic hydrocarbons via ωC_2. The positive correlations of the ^{13}C values of C_2 with mass ratios of $C_2/\omega C_2$ ($R^2 \geq 0.39$) and C_2/kC_3 ($R^2 \geq 0.37$) during the LCD were observed, whereas such robust relations only with $C_2/\omega C_2$ ($R^2 \geq 0.47$) rather than C_2/kC_3 ($R^2 \geq 0.01$) before the LCD were observed (Fig. 9). These results imply that the effect of photochemical decomposition of higher diacid homologues on C_2 before the LCD was minor, which was consistent with the discussions in Section 3.3. The isotopic values of diacids followed the order of $C_2 > C_3 > C_4$ in each period (Fig. 7), primarily because diacids containing more carbon numbers may be more reactive to oxidants such as O_3 and OH radicals in the atmosphere (Aggarwal and Kawamura, 2008). On the other hand, the removal of CO_2/CO in the processes of C_3 and C_4 reacting with atmospheric oxidants can generate more ^{13}C-enriched C_2 due to the KIEs (Wang and Kawamura, 2006). The isotopic values of C_9 ranged from $-25.2‰$ to $-29.8‰$ before the LCD, whose difference was less distinguished than those of C_2-C_4 (Table 3). It is worth noting that the $\delta^{13}C$ values of organic species from marine plankton ($-20‰$) are higher than those from terrestrial higher plants (C_3 plants: $-27‰$). The $\delta^{13}C$ values of C_9 and the strong correlation of C_9 with levoglucosan before the LCD as discussed above indicate that biomass burning emitting unsaturated fatty acids and subsequent aqueous oxidation was an important contributor to C_9 in Jinan during the wintertime. The most negative $\delta^{13}C$ value among the identified organic species was tPh throughout the entire period, whose $\delta^{13}C$ value ($-35.4 \pm 3.1‰$) was approximately equal to that ($-35.2 \pm 5.3‰$) in Liaocheng (Meng et al., 2020) and lighter than that ($-33.5 \pm 3.4‰$) in Beijing (Zhao et al., 2018) of China where the primary emissions from the combustion of plastic wastes is an essential source of tPh. Moreover, the $\delta^{13}C$ value of tPh was negatively or poorly correlated with the ratio of tPh/diacids before and during the LCD, respectively (Fig. 9). These results suggest that the primary sources of plastic wastes burning exerted a significant impact on tPh in the atmosphere of Jinan.

Similarly, the $\delta^{13}C$ value of oxoacids increases as carbon number decreases (Table 3, Fig. 7). ωC_2 has the highest $\delta^{13}C$ value, followed by Pyr, and ωC_3 before and during the LCD. The more pronounced enhancement of $\delta^{13}C$ values in C_2 and ωC_2 in each period suggests that C_2 in Jinan aerosols was mainly originated from aqueous oxidation of ωC_2 (Meng et al., 2020). However, the lighter isotope (^{12}C) was more enriched in ωC_2 than both Gly and mGly (Table 3) in each period. ωC_2 is largely derived from the photochemical oxidation of organic precursors such as α-dicarbonyls and acetic acid (Carlton et al., 2007). ^{12}C can be preferentially accumulated in the products in the non-reversible chemical processes (Wang et al., 2012), resulting in the lighter $\delta^{13}C$ values of ωC_2 than its precursors. mGly was less enriched in ^{13}C than Gly (Table 3, Fig. 7) in

each period, which was attributed to the lower vapor pressure and higher carbon numbers of mGly that may lead to the weaker isotopic fractionation (Zhang et al., 2016).

3.5.2 Difference in $\delta^{13}C$ values before and during the LCD

It is well established that the ^{13}C values of diacids and related compounds become isotopically heavier in the aging process of organic aerosols (Pavuluri and Kawamura, 2016; Zhang et al., 2016). As mentioned above, the ratios of C_2/Gly, $C_2/mGly$, and $C_2/diacids$ are usually considered significant proxies to evaluate the aging of organic aerosols. These ratios exhibited strong correlations with the ^{13}C values of C_2 in each period ($R^2 > 0.4$, Fig. 9), indicating the production of more ^{13}C-enriched C_2 during the aging processes. The less depletion of ^{13}C in C_2 of aged organic aerosols conformed to the actual secondary KIE on activated H-atom abstraction by OH radicals rather than to the mass dependence of collision frequencies in the gas phase (Enami et al., 2015). Organic species can react with OH radicals and other atmospheric oxidants in the atmospheric oxidation reactions, which result in the removal of CO_2/CO containing ^{12}C and cause the oxidation products more enriched with the heavier isotope ^{13}C (Narukawa et al., 1999). Therefore, the ^{13}C values of major diacids and the related compounds during the LCD were less negative than those before the LCD, again demonstrating that the photochemical oxidation was promoted during the LCD because of the higher temperature and O_3 concentration under the more clear sky conditions.

3.6 Comparison of the source fingerprinting before and during the LCD

To further investigate the crucial sources of diacids and related compounds, positive matrix factorization (PMF) was adopted. Detailed information about PMF analysis was described in Text S3. The model stability of the five-factor solution and error estimation diagnostics were detailed in Table S4 and Table S5, respectively. The PMF-resolved source profiles for the five factors before and during the LCD were shown in Fig. 10. Before the LCD, C_2, C_3, ωC_2, mGly, WSOC, NO_3^-, SO_4^{2-}, and NH_4^+ exhibited the relatively higher loadings in the first factor (Fig. 10a). SO_4^{2-} is a representative product of secondary oxidation in the aqueous phase, thus the first factor was considered the sources from aqueous phase oxidation. The second factor was characterized by the stronger loadings of C_3, Ph, and EC. Ph is generated from the photochemical oxidation of polycyclic aromatic hydrocarbons (e.g., naphthalene) that are primarily emitted from the domestic coal combustion in China's megacities (Zhao et al., 2018), thus the second factor was categorized as a coal combustion source. O_3 had been confirmed to be a reliable proxy for photochemical oxidation, thus the robust relationships of O_3, α-dicarbonyls, and ωC_2 with the third factor indicated the contribution of photochemical oxidation. The fourth factor was significantly associated with Mg^{2+} and Ca^{2+}, which represented the dust sources. As an important indicator of biomass burning, levoglucosan was strongly correlated with C_4, C_9, Pyr, and EC in the fifth factor, suggesting the contribution of biomass burning.

During the LCD, the first factor was dominated by O_3, major diacids, and α-dicarbonyls (Fig. 10b), which represented photochemical oxidation dominated by O_3. The second factor was strongly correlated with C_2, C_4, WSOC, NO_3^-, SO_4^{2-}, and NH_4^+, suggesting a significant contribution of aqueous oxidation. Levoglucosan, C_9, Pyr, and OC presented the stronger loadings in the third factor, indicating the sources from biomass burning. Mg^{2+} and Ca^{2+} exhibited strong correlations with the fourth factor, suggesting the sources from dust. Ph and EC presented the strong correlations with the fifth factor, representing a coal combustion source.

The PMF-resolved relative contributions to the detected species before and during the LCD were presented in Fig. 10c and Fig. 10d, respectively. The aqueous oxidation made the greatest contribution (46.1%) to C_2 and related compounds before the LCD, while it accounted for only 16.1% in the total identified sources during the LCD. The photochemical oxidation dominated by O_3 contributed the largest percentage (50.3%) to the total identified sources, confirming that such a source exerted a leading role in the formation of homologous diacids during the LCD, which was agreement with the results as discussed above. The contribution of biomass burning increased from 10.2% before the LCD to 14.2% during the LCD.

However, the contribution of coal combustion decreased from 17.4% before the LCD to 7.9% during the LCD, largely because of the decreased usage of coal for industry during the LCD.

4 Summary and conclusions

To explore the impact of LCD on the SOA, $PM_{2.5}$ aerosols from Jinan, a megacity in East China, before and during the LCD were analyzed for OC, EC, WSOC, inorganic ions, diacids, oxoacids, and α-dicarbonyls. Due to the sharp dropping of human activities, the air pollutants including $PM_{2.5}$, PM_{10}, CO, SO_2, and NO_2 during the LCD reduced by 39.3–62.4% than those before the LCD. However, the O_3 concentration increased by 1.3 times synchronously during the LCD. The concentrations of diacids and oxoacids during the LCD exhibited upward trends, while α-dicarbonyls during the LCD was almost equal to that before the LCD. C_2 before the LCD was significantly derived from the acid-catalyzed aqueous phase oxidation of organic precursors emitted from biomass burning where RH and LWC played a significant role. However, C_2 during the LCD was dominantly generated from photochemical degradation of longer-chain homologous diacids driven by stronger solar radiation and higher O_3 concentration rather than higher temperature. The $\delta^{13}C$ values of major detected diacids were more positive during the LCD than before the LCD, with the largest value (-20 ± 2.5‰) for C_2 and the smallest (-35 ± 3.1‰) for tPh. The ratios of C_2/Gly, C_2/mGly, and C_2/diacids exhibited strong correlations with ^{13}C values of C_2, indicating the more enriched ^{13}C in C_2 during the aging processes of organic aerosols. The molecular distributions of diacid homologues and PMF results suggest that TDOCs in Jinan were primarily derived from the aqueous mechanisms of organic precursors emitted from coal combustion and biomass burning before the LCD, while these species were principally derived from the O_3-dominated photochemical pathways during the LCD.

Data availability. The data in this study are available at: https://doi.org/10.5281/zenodo.7533247 (Meng et al., 2023).

Author contribution. PF designed the study. WY, LY, HT, and CM carried out the experiments and performed the data analysis. JM prepared the manuscript with contributions from all co-authors.

Competing interests. The authors have the following competing interests: One of the coauthors, Prof. Kimitaka Kawamura is one of the editorial members of this journal.

Acknowledgments. This work was supported by the National Natural Science Foundation of China (Grant No. 42177083), the Natural Science Foundation of Shandong Province (Grant No. ZR2020MD113), the Junior Faculty Support Program for Scientific and Technological Innovations in Shandong Provincial Higher Education Institutions (2021KJ085), and the Open Funds of State Key Laboratory of Loess and Quaternary Geology, Institute of Earth Environment, Chinese Academy of Sciences (Grant No. SKLLOG2020).

References

Aggarwal, S. G. and Kawamura, K.: Molecular distributions and stable carbon isotopic compositions of dicarboxylic acids and related compounds in aerosols from Sapporo, Japan: Implications for photochemical aging during long-range atmospheric transport, J. Geophys. Res. Atmos., 113, D14301, 10.1029/2007jd009365, 2008.

Andreae, M. O.: Soot Carbon and Excess Fine Potassium: Long-Range Transport of Combustion-Derived Aerosols, Science, 220, 1148, 1983.

Bao, R. and Zhang, A.: Does lockdown reduce air pollution? Evidence from 44 cities in northern China, Sci. Total Environ.,731, 139052, https://doi.org/10.1016/j.scitotenv.2020.139052, 2020.

Bikkina, S., Kawamura, K., and Miyazaki, Y.: Latitudinal distributions of atmospheric dicarboxylic acids, oxocarboxylic

acids, and α-dicarbonyls over the western North Pacific: Sources and formation pathways, J. Geophys. Res. Atmos., 120, 5010-5035, 10.1002/2014jd022235, 2015.

Bikkina, S., Kawamura, K., Sakamoto, Y., and Hirokawa, J.: Low molecular weight dicarboxylic acids, oxocarboxylic acids and α-dicarbonyls as ozonolysis products of isoprene: Implication for the gaseous-phase formation of secondary organic aerosols, Sci. Total Environ., 769, 144472, https://doi.org/10.1016/j.scitotenv.2020.144472, 2021.

Bilde, M., Barsanti, K., Booth, M., Cappa, C. D., Donahue, N. M., Emanuelsson, E. U., McFiggans, G., Krieger, U. K., Marcolli, C., Topping, D., Ziemann, P., Barley, M., Clegg, S., Dennis-Smither, B., Hallquist, M., Hallquist, Å. M., Khlystov, A., Kulmala, M., Mogensen, D., Percival, C. J., Pope, F., Reid, J. P., Ribeiro da Silva, M. A. V., Rosenoern, T., Salo, K., Soonsin, V. P., Yli-Juuti, T., Prisle, N. L., Pagels, J., Rarey, J., Zardini, A. A., and Riipinen, I.: Saturation Vapor Pressures and Transition Enthalpies of Low-Volatility Organic Molecules of Atmospheric Relevance: From Dicarboxylic Acids to Complex Mixtures, Chem. Rev., 115, 4115-4156, 10.1021/cr5005502, 2015.

Cao, F., Zhang, S.-C., Kawamura, K., Liu, X., Yang, C., Xu, Z., Fan, M., Zhang, W., Bao, M., Chang, Y., Song, W., Liu, S., Lee, X., Li, J., Zhang, G., and Zhang, Y.-L.: Chemical characteristics of dicarboxylic acids and related organic compounds in PM2.5 during biomass-burning and non-biomass-burning seasons at a rural site of Northeast China, Environ. Pollut., 231, 654-662, https://doi.org/10.1016/j.envpol.2017.08.045, 2017.

Carlton, A. G., Turpin, B. J., Lim, H.-J., Altieri, K. E., and Seitzinger, S.: Link between isoprene and secondary organic aerosol (SOA): Pyruvic acid oxidation yields low volatility organic acids in clouds, Geophys. Res. Lett., 33, L06822, 10.1029/2005gl025374, 2006.

Carlton, A. G., Turpin, B. J., Altieri, K. E., Seitzinger, S., Reff, A., Lim, H.-J., and Ervens, B.: Atmospheric oxalic acid and SOA production from glyoxal: Results of aqueous photooxidation experiments, Atmos. Environ., 41, 7588-7602, http://dx.doi.org/10.1016/j.atmosenv.2007.05.035, 2007.

Cheng, C., Wang, G., Meng, J., Wang, Q., Cao, J., Li, J., and Wang, J.: Size-resolved airborne particulate oxalic and related secondary organic aerosol species in the urban atmosphere of Chengdu, China, Atmos. Res., 161–162, 134-142, http://dx.doi.org/10.1016/j.atmosres.2015.04.010, 2015.

Chow, J. C., Watson, J. G., Chen, L. W. A., Arnott, W. P., Moosmüller, H., and Fung, K.: Equivalence of Elemental Carbon by Thermal/Optical Reflectance and Transmittance with Different Temperature Protocols, Environ. Sci. Technol., 38, 4414-4422, 10.1021/es034936u, 2004.

Deshmukh, D. K., Mozammel Haque, M., Kawamura, K., and Kim, Y.: Dicarboxylic acids, oxocarboxylic acids and α-dicarbonyls in fine aerosols over central Alaska: Implications for sources and atmospheric processes, Atmos. Res., 202, 128-139, https://doi.org/10.1016/j.atmosres.2017.11.003, 2018.

Ding, Z., Du, W., Wu, C., Cheng, C., Meng, J., Li, D., Ho, K., Zhang, L., and Wang, G.: Summertime atmospheric dicarboxylic acids and related SOA in the background region of Yangtze River Delta, China: Implications for heterogeneous reaction of oxalic acid with sea salts, Sci. Total Environ., 757, 143741, https://doi.org/10.1016/j.scitotenv.2020.143741, 2021.

Enami, S., Hoffmann, M. R., and Colussi, A. J.: Stepwise Oxidation of Aqueous Dicarboxylic Acids by Gas-Phase OH Radicals, J. Phys., Chem. Lett., 6, 527-534, 10.1021/jz502432j, 2015.

Ervens, B., Feingold, G., Frost, G. J., and Kreidenweis, S. M.: A modeling study of aqueous production of dicarboxylic acids: 1. Chemical pathways and speciated organic mass production, J. Geophys. Res., 109, D15205, 10.1029/2003jd004387, 2004.

Ervens, B., Turpin, B. J., and Weber, R. J.: Secondary organic aerosol formation in cloud droplets and aqueous particles (aqSOA): a review of laboratory, field and model studies, Atmos. Chem. Phys., 11, 11069-11102, 10.5194/acp-11-11069-2011, 2011.

Fountoukis, C., and Nenes, A.: ISORROPIA II: a computationally efficient thermodynamic equilibrium model for K^+–Ca^{2+}–Mg^{2+}–NH_4^+–Na^+–SO_4^{2-}–NO_3^-–Cl^-–H_2O aerosols, Atmos. Chem. Phys., 7, 4639-4659, 10.5194/acp-7-4639-2007, 2007.

530   Fu, P., Kawamura, K., Usukura, K., and Miura, K.: Dicarboxylic acids, ketocarboxylic acids and glyoxal in the marine aerosols collected during a round-the-world cruise, Marine Chemistry, 148, 22-32, http://dx.doi.org/10.1016/j.marchem.2012.11.002, 2013.

Fu, T.-M., Jacob, D. J., Wittrock, F., Burrows, J. P., Vrekoussis, M., and Henze, D. K.: Global budgets of atmospheric glyoxal and methylglyoxal, and implications for formation of secondary organic aerosols, J. Geophys. Res., 113,
535   D15303, 10.1029/2007jd009505, 2008.

Gao, S., Hegg, D. A., Hobbs, P. V., Kirchstetter, T. W., Magi, B. I., and Sadilek, M.: Water-soluble organic components in aerosols associated with savanna fires in southern Africa: Identification, evolution, and distribution, J. Geophys. Res. Atmos., 108, 8491, 10.1029/2002jd002324, 2003.

Gligorovski, S., Grgić, I., Net, S., Böge, O., Iinuma, Y., Kahnt, A., Scheinhardt, S., Herrmann, H., and Wortham, H.:
540   Light-induced multiphase chemistry of gas phase ozone on aqueous pyruvic and oxalic acids: Aerosol chamber study, AGU Fall Meeting Abstracts, 2010.

Ho, K. F., Cao, J. J., Lee, S. C., Kawamura, K., Zhang, R. J., Chow, J. C., and Watson, J. G.: Dicarboxylic acids, ketocarboxylic acids, and dicarbonyls in the urban atmosphere of China, J. Geophys. Res. Atmos., 112, D22S27, 10.1029/2006jd008011, 2007.

545   Hu, W., Hu, M., Hu, W. W., Zheng, J., Chen, C., Wu, Y., and Guo, S.: Seasonal variations in high time-resolved chemical compositions, sources, and evolution of atmospheric submicron aerosols in the megacity Beijing, Atmos. Chem. Phys., 17, 9979-10000, 10.5194/acp-17-9979-2017, 2017.

Huang, X., Ding, A., Gao, J., Zheng, B., Zhou, D., Qi, X., Tang, R., Wang, J., Ren, C., Nie, W., Chi, X., Xu, Z., Chen, L., Li, Y., Che, F., Pang, N., Wang, H., Tong, D., Qin, W., Cheng, W., Liu, W., Fu, Q., Liu, B., Chai, F., Davis, S. J.,
550   Zhang, Q., and He, K.: Enhanced secondary pollution offset reduction of primary emissions during COVID-19 lockdown in China, Natl. Sci. Rev., 10.1093/nsr/nwaa137, 2020.

Jang, M., Czoschke, N. M., Lee, S., and Kamens, R. M.: Heterogeneous Atmospheric Aerosol Production by Acid-Catalyzed Particle-Phase Reactions, Science, 298, 814, 2002.

Kawamura, K. and Bikkina, S.: A review of dicarboxylic acids and related compounds in atmospheric aerosols: Molecular
555   distributions, sources and transformation, Atmos. Res., 170, 140-160, http://dx.doi.org/10.1016/j.atmosres.2015.11.018, 2016.

Kawamura, K. and Kaplan, I. R.: Motor exhaust emissions as a primary source for dicarboxylic acids in Los Angeles ambient air, Environ. Sci. Technol., 21, 105-110, 10.1021/es00155a014, 1987.

Kawamura, K. and Usukura, K.: Distributions of low molecular weight dicarboxylic acids in the North Pacific aerosol
560   samples, J. Oceano., 49, 271-283, 10.1007/bf02269565, 1993.

Kawamura, K. and Watanabe, T.: Determination of Stable Carbon Isotopic Compositions of Low Molecular Weight Dicarboxylic Acids and Ketocarboxylic Acids in Atmospheric Aerosol and Snow Samples, Anal. Chem., 76, 5762-5768, 10.1021/ac049491m, 2004.

Le, T., Wang, Y., Liu, L., Yang, J., Yung, Y. L., Li, G., and Seinfeld, J. H.: Unexpected air pollution with marked emission
565   reductions during the COVID-19 outbreak in China, Science, eabb7431, 10.1126/science.abb7431, 2020.

Li, L., Li, Q., Huang, L., Wang, Q., Zhu, A., Xu, J., Liu, Z., Li, H., Shi, L., Li, R., Azari, M., Wang, Y., Zhang, X., Liu, Z., Zhu, Y., Zhang, K., Xue, S., Ooi, M. C. G., Zhang, D., and Chan, A.: Air quality changes during the COVID-19 lockdown over the Yangtze River Delta Region: An insight into the impact of human activity pattern changes on air pollution variation, Sci. Total Environ., 732, 139282, https://doi.org/10.1016/j.scitotenv.2020.139282, 2020.

570   Li, Z., Zhou, R., Wang, Y., Wang, G., Chen, M., Li, Y., Wang, Y., Yi, Y., Hou, Z., Guo, Q., and Meng, J.: Characteristics and sources of amine-containing particles in the urban atmosphere of Liaocheng, a seriously polluted city in North China during the COVID-19 outbreak, Environ. Pollut., 289, 117887, https://doi.org/10.1016/j.envpol.2021.117887, 2021.

Lim, Y. B., Tan, Y., and Turpin, B. J.: Chemical insights, explicit chemistry, and yields of secondary organic aerosol from
575   OH radical oxidation of methylglyoxal and glyoxal in the aqueous phase, Atmos. Chem. Phys., 13, 8651-8667, 10.5194/acp-13-8651-2013, 2013.

Liu, J., Zhou, S., Zhang, Z., Kawamura, K., Zhao, W., Wang, X., Shao, M., Jiang, F., Liu, J., Sun, X., Hang, J., Zhao, J., Pei, C., Zhang, J., and Fu, P.: Characterization of dicarboxylic acids, oxoacids, and α-dicarbonyls in PM2.5 within the urban boundary layer in southern China: Sources and formation pathways, Environ. Pollut., 285, 117185,
580   https://doi.org/10.1016/j.envpol.2021.117185, 2021.

Lv, S., Wang, F., Wu, C., Chen, Y., Liu, S., Zhang, S., Li, D., Du, W., Zhang, F., Wang, H., Huang, C., Fu, Q., Duan, Y., and Wang, G.: Gas-to-Aerosol Phase Partitioning of Atmospheric Water-Soluble Organic Compounds at a Rural Site in China: An Enhancing Effect of NH3 on SOA Formation, Environ. Sci. Technol., 56, 3915-3924, 10.1021/acs.est.1c06855, 2022.

585   Meng, J., Liu, X., Hou, Z., Yi, Y., Yan, L., Li, Z., Cao, J., Li, J., and Wang, G.: Molecular characteristics and stable carbon isotope compositions of dicarboxylic acids and related compounds in the urban atmosphere of the North China Plain: Implications for aqueous phase formation of SOA during the haze periods, Sci. Total Environ., 705, 135256, https://doi.org/10.1016/j.scitotenv.2019.135256, 2020.

Meng, J., Li, Z., Zhou, R., Chen, M., Li, Y., Yi, Y., Ding, Z., Li, H., Yan, L., Hou, Z., and Wang, G.: Enhanced
590   photochemical formation of secondary organic aerosols during the COVID-19 lockdown in Northern China, Sci. Total Environ., 758, 143709, https://doi.org/10.1016/j.scitotenv.2020.143709, 2021.

Meng, J., Wang, G., Hou, Z., Liu, X., Wei, B., Wu, C., Cao, C., Wang, J., Li, J., Cao, J., Zhang, E., Dong, J., Liu, J., Ge, S., and Xie, Y.: Molecular distribution and stable carbon isotopic compositions of dicarboxylic acids and related SOA from biogenic sources in the summertime atmosphere of Mt. Tai in the North China Plain, Atmos. Chem. Phys., 18,
595   15069-15086, 10.5194/acp-18-15069-2018, 2018.

Miyazaki, Y., Aggarwal, S. G., Singh, K., Gupta, P. K., and Kawamura, K.: Dicarboxylic acids and water-soluble organic carbon in aerosols in New Delhi, India, in winter: Characteristics and formation processes, J. Geophys. Res. Atmos., 114, D19206, 10.1029/2009jd011790, 2009.

Mochizuki, T., Kawamura, K., Miyazaki, Y., Wada, R., Takahashi, Y., Saigusa, N., and Tani, A.: Secondary formation of
600   oxalic acid and related organic species from biogenic sources in a larch forest at the northern slope of Mt. Fuji, Atmos. Environ., 166, 255-262, https://doi.org/10.1016/j.atmosenv.2017.07.028, 2017.

Narukawa, M., Kawamura, K., Takeuchi, N., and Nakajima, T.: Distribution of dicarboxylic acids and carbon isotopic compositions in aerosols from 1997 Indonesian forest fires, Geophys. Res. Lett., 26, 3101-3104, https://doi.org/10.1029/1999GL010810, 1999.

605   Pavuluri, C. M. and Kawamura, K.: Enrichment of ^{13}C in diacids and related compounds during photochemical processing of aqueous aerosols: New proxy for organic aerosols aging, Sci. Rep., 6, 36467, 10.1038/srep36467, 2016.

Rinaldi, M., Decesari, S., Carbone, C., Finessi, E., Fuzzi, S., Ceburnis, D., O'Dowd, C. D., Sciare, J., Burrows, J. P., Vrekoussis, M., Ervens, B., Tsigaridis, K., and Facchini, M. C.: Evidence of a natural marine source of oxalic acid and a possible link to glyoxal, J. Geophys. Res. Atmos., 116, n/a-n/a, 10.1029/2011jd015659, 2011.

610   Shen, M., Ho, K. F., Dai, W., Liu, S., Zhang, T., Wang, Q., Meng, J., Chow, J. C., Watson, J. G., Cao, J., and Li, J.: Distribution and stable carbon isotopic composition of dicarboxylic acids, ketocarboxylic acids and α-dicarbonyls in fresh and aged biomass burning aerosols, Atmos. Chem. Phys., 22, 7489-7504, 10.5194/acp-22-7489-2022,

2022.

Shi, Z., Song, C., Liu, B., Lu, G., Xu, J., Van Vu, T., Elliott Robert, J. R., Li, W., Bloss William, J., and Harrison Roy, M.: Abrupt but smaller than expected changes in surface air quality attributable to COVID-19 lockdowns, Sci. Adv.,7, eabd6696, 10.1126/sciadv.abd6696, 2021.

Sorathia, F., Rajput, P., and Gupta, T.: Dicarboxylic acids and levoglucosan in aerosols from Indo-Gangetic Plain: Inferences from day night variability during wintertime, Sci. Total Environ., 624, 451-460, https://doi.org/10.1016/j.scitotenv.2017.12.124, 2018.

Surratt, J. D., Lewandowski, M., Offenberg, J. H., Jaoui, M., Kleindienst, T. E., Edney, E. O., and Seinfeld, J. H.: Effect of Acidity on Secondary Organic Aerosol Formation from Isoprene, Environ. Sci. Technol., 41, 5363-5369, 10.1021/es0704176, 2007.

Sun, Y., Wang, Z., Fu, P., Yang, T., Jiang, Q., Dong, H., Li, J., and Jia, J.: Aerosol composition, sources and processes during wintertime in Beijing, China, Atmos. Chem. Phys., 13, 4577-4592, 10.5194/acp-13-4577-2013, 2013.

Wang, G., Cheng, C., Meng, J., Huang, Y., Li, J., and Ren, Y.: Field observation on secondary organic aerosols during Asian dust storm periods: Formation mechanism of oxalic acid and related compounds on dust surface, Atmos. Environ., 113, 169-176, http://dx.doi.org/10.1016/j.atmosenv.2015.05.013, 2015.

Wang, G., Xie, M., Hu, S., Gao, S., Tachibana, E., and Kawamura, K.: Dicarboxylic acids, metals and isotopic compositions of C and N in atmospheric aerosols from inland China: implications for dust and coal burning emission and secondary aerosol formation, Atmos. Chem. Phys., 10, 6087-6096, 10.5194/acp-10-6087-2010, 2010.

Wang, G., Kawamura, K., Cheng, C., Li, J., Cao, J., Zhang, R., Zhang, T., Liu, S., and Zhao, Z.: Molecular Distribution and Stable Carbon Isotopic Composition of Dicarboxylic Acids, Ketocarboxylic Acids, and α-Dicarbonyls in Size-Resolved Atmospheric Particles From Xiꞌan City, China, Environ. Sci. Technol., 46, 4783-4791, 10.1021/es204322c, 2012.

Wang, G., Zhang, R., Gomez, M. E., Yang, L., Levy Zamora, M., Hu, M., Lin, Y., Peng, J., Guo, S., Meng, J., Li, J., Cheng, C., Hu, T., Ren, Y., Wang, Y., Gao, J., Cao, J., An, Z., Zhou, W., Li, G., Wang, J., Tian, P., Marrero-Ortiz, W., Secrest, J., Du, Z., Zheng, J., Shang, D., Zeng, L., Shao, M., Wang, W., Huang, Y., Wang, Y., Zhu, Y., Li, Y., Hu, J., Pan, B., Cai, L., Cheng, Y., Ji, Y., Zhang, F., Rosenfeld, D., Liss, P. S., Duce, R. A., Kolb, C. E., and Molina, M. J.: Persistent sulfate formation from London Fog to Chinese haze, P. Natl. Acad. Sci. USA, 113, 13630-13635, 10.1073/pnas.1616540113, 2016.

Wang, H. and Kawamura, K.: Stable carbon isotopic composition of low-molecular-weight dicarboxylic acids and ketoacids in remote marine aerosols, J. Geophys. Res. Atmos., 111, https://doi.org/10.1029/2005JD006466, 2006.

Wang, H., Huang, C., Tao, W., Gao, Y., Wang, S., Jing, S., Wang, W., Yan, R., Wang, Q., An, J., Tian, J., Hu, Q., Lou, S., Pöschl, U., Cheng, Y., and Su, H.: Seasonality and reduced nitric oxide titration dominated ozone increase during COVID-19 lockdown in eastern China, npj Climate and Atmospheric Science, 5, 24, 10.1038/s41612-022-00249-3, 2022.

Wang, J., Wang, G., Wu, C., Li, J., Cao, C., Li, J., Xie, Y., Ge, S., Chen, J., Zeng, L., Zhu, T., Zhang, R., and Kawamura, K.: Enhanced aqueous-phase formation of secondary organic aerosols due to the regional biomass burning over North China Plain, Environ. Pollut., 256, 113401, https://doi.org/10.1016/j.envpol.2019.113401, 2020a.

Wang, P., Chen, K., Zhu, S., Wang, P., and Zhang, H.: Severe air pollution events not avoided by reduced anthropogenic activities during COVID-19 outbreak, Resour. Conserv. Recy., 158, 104814, https://doi.org/10.1016/j.resconrec.2020.104814, 2020b.

Warneck, P.: In-cloud chemistry opens pathway to the formation of oxalic acid in the marine atmosphere, Atmos. Environ., 37, 2423-2427, http://dx.doi.org/10.1016/S1352-2310(03)00136-5, 2003.

Wu, J., Bei, N., Hu, B., Liu, S., Wang, Y., Shen, Z., Li, X., Liu, L., Wang, R., Liu, Z., Cao, J., Tie, X., Molina, L. T., and Li,

G.: Aerosol–photolysis interaction reduces particulate matter during wintertime haze events, P. Natl. Acad. Sci. USA, 117, 9755-9761, 10.1073/pnas.1916775117, 2020.

Xu, B., Zhang, G., Gustafsson, Ö., Kawamura, K., Li, J., Andersson, A., Bikkina, S., Kunwar, B., Pokhrel, A., Zhong, G., Zhao, S., Li, J., Huang, C., Cheng, Z., Zhu, S., Peng, P., and Sheng, G.: Large contribution of fossil-derived components to aqueous secondary organic aerosols in China, Nat. Commun., 13, 5115, 10.1038/s41467-022-32863-3, 2022.

Yu, Q., Chen, J., Cheng, S., Qin, W., Zhang, Y., Sun, Y., and Ahmad, M.: Seasonal variation of dicarboxylic acids in PM2.5 in Beijing: Implications for the formation and aging processes of secondary organic aerosols, Sci. Total Environ., 763, 142964, https://doi.org/10.1016/j.scitotenv.2020.142964, 2021.

Yu, Q., Chen, J., Qin, W., Cheng, S., Zhang, Y., Ahmad, M., and Ouyang, W.: Characteristics and secondary formation of water-soluble organic acids in PM1, PM2.5 and PM10 in Beijing during haze episodes, Sci. Total Environ., 669, 175-184, https://doi.org/10.1016/j.scitotenv.2019.03.131, 2019.

Zhang, Y., Kawamura, K., Cao, F., and Lee, M.: Stable carbon isotopic compositions of low-molecular-weight dicarboxylic acids, oxocarboxylic acids, α-dicarbonyls, and fatty acids: Implications for atmospheric processing of organic aerosols, J. Geophys. Res. Atmos., 121, 3707-3717, 10.1002/2015jd024081, 2016.

Zhang, R., Wang, G., Guo, S., Zamora, M. L., Ying, Q., Lin, Y., Wang, W., Hu, M., and Wang, Y.: Formation of Urban Fine Particulate Matter, Chemical Reviews, 115, 3803-3855, 10.1021/acs.chemrev.5b00067, 2015.

Zhao, W., Kawamura, K., Yue, S., Wei, L., Ren, H., Yan, Y., Kang, M., Li, L., Ren, L., Lai, S., Li, J., Sun, Y., Wang, Z., and Fu, P.: Molecular distribution and compound-specific stable carbon isotopic composition of dicarboxylic acids, oxocarboxylic acids and α-dicarbonyls in PM$_{2.5}$ from Beijing, China, Atmos. Chem. Phys., 18, 2749-2767, 10.5194/acp-18-2749-2018, 2018.

Zhao, W., Ren, H., Kawamura, K., Du, H., Chen, X., Yue, S., Xie, Q., Wei, L., Li, P., Zeng, X., Kong, S., Sun, Y., Wang, Z., and Fu, P.: Vertical distribution of particle-phase dicarboxylic acids, oxoacids and α-dicarbonyls in the urban boundary layer based on the 325 m tower in Beijing, Atmos. Chem. Phys., 20, 10331-10350, 10.5194/acp-20-10331-2020, 2020.

Zhong, H., Huang, R., Chang, Y., Duan, J., Lin, C., and Chen, Y.: Enhanced formation of secondary organic aerosol from photochemical oxidation during the COVID-19 lockdown in a background site in Northwest China, Sci. Total Environ., 778, 144947, https://doi.org/10.1016/j.scitotenv.2021.144947, 2021.

685 **Table 1. Meteorological parameters, liquid water content (LWC) of aerosol, in-situ pH (pH_{is}), and chemical compositions of $PM_{2.5}$ before (January 6 – 23, 2020) and during the lockdown (LCD) (January 31 – February 17, 2020) in Jinan, China.**

	Before the LCD (n=36)	During the LCD (n=36)	Whole period (n=72)
I. Meteorological parameters			
Temperature (^{o}C)	0.07 ± 5.9 (-16.5–12.6)	6.8 ± 5.2 (-3.4–16.1)	3.4 ± 6.5 (-16–16)
Relative humidity (%)	52.2 ± 10.2 (29.8–86.9)	38.8 ± 17.8 (16.8– 85.3)	45.5 ± 15.9 (16.8–86.9)
Solar radiation (W m^{-2})	164 ± 69.9 (31.5–282)	255 ± 117 (17.5–423)	209 ± 106 (17.5–423)
Wind speed (m s^{-1})	3.0 ± 0.7 (1.6–4.6)	3.7 ± 1.1 (1.2–6.6)	3.3 ± 1.0 (1.2–6.6)
II. Gaseous pollutants (μg m^{-3})			
SO_2	22.7 ± 8.9 (8.3–49.4)	13.8 ± 4.9 (4.9–28.8)	18.3 ± 8.5 (4.9–49.4)
NO_2	55.9 ± 11.6 (37.9–81.2)	21.1 ± 5.9 (9.3–33.5)	38.5 ± 19.8 (9.3–81.2)
CO	1.6 ± 0.3 (0.9–2.5)	0.9 ± 0.2 (0.5–1.6)	1.3 ± 0.5 (0.5–2.5)
O_3	28.9 ± 18.2 (5.3–74.4)	66.3 ± 21.0 (25.4–109)	47.6 ± 27.1 (5.3–109)
III. Inorganic ions (μg m^{-3})			
K^+	1.0 ± 0.1 (0.9–1.7)	1.3 ± 0.6 (0.5–2.9)	1.1 ± 0.4 (0.5–2.9)
Na^+	0.3 ± 0.1 (0.1–0.6)	0.2 ± 0.1 (0.1–0.8)	0.2 ± 0.1 (0.1–0.8)
Ca^{2+}	0.4 ± 0.2 (0.1–0.9)	0.5 ± 0.2 (0.2–1.1)	0.5 ± 0.2 (0.1–1.1)
Mg^{2+}	0.1 ± 0.03 (0–0.1)	0.1 ± 0.1 (0.1–0.4)	0.1 ± 0.1 (0–0.4)
NH_4^+	11.5 ± 5.7 (4.4–26.1)	7.7 ± 4.7 (0.4–15.6)	9.6 ± 5.5 (0.4–26.1)
NO_3^-	19.3 ± 11.0 (5.4–48.6)	9.6 ± 4.9 (1.2–18.2)	14.4 ± 9.7 (1.2–48.6)
SO_4^{2-}	12.8 ± 6.9 (3.8–30.7)	9.4 ± 5.3 (1.1–17.7)	11.1 ± 6.4 (1.1–30.7)
SNA[a]	43.6 ± 23.4 (14.6–105)	26.7 ± 14.6 (2.8–49.8)	35.1 ± 21.1 (2.8–105)
Subtotal	48.7 ± 24.3 (17.9–113)	34.5 ± 17.5 (6.1–67.0)	41.6 ± 22.2 (6.1–113)
IV. Carbonaceous species (μg m^{-3})			
EC	4.3 ± 2.4 (0.9–11.2)	1.9 ± 1.0 (0.3–3.8)	3.1 ± 2.2 (0.3–11.2)
OC	10.3 ± 3.0 (5.2–18.8)	6.4 ± 2.6 (2.0–11.2)	8.3 ± 3.4 (2.0–18.8)
WSOC	3.9 ± 1.9 (1.2–10.4)	3.2 ± 1.4 (1.0–7.0)	3.5 ± 1.7 (1.0–10.4)
OC/EC	2.9 ± 1.3 (1.5–6.9)	4.0 ± 1.5 (2.4–8.4)	3.5 ± 1.5 (1.5–8.4)
WSOC/OC	0.4 ± 0.1 (0.2–0.7)	0.5 ± 0.1 (0.3–0.8)	0.4 ± 0.1 (0.2–0.8)
V. Other species			
$PM_{2.5}$ (μg m^{-3})	106 ± 45.2 (35.0–202)	55.5 ± 29.4 (10.0–111)	80.8 ± 45.6 (10.0–202)
PM_{10} (μg m^{-3})	147 ± 57.9 (37.9–285)	71.6 ± 32.7 (19.0–129)	109 ± 60.1 (19.0–285)
Levoglucosan (ng m^{-3})	141 ± 70.2 (49.9–370)	102 ± 29.5 (60.7–186)	121 ± 57.0 (49.9–370)
pH_{is}	3.2 ± 3.0 (2.3–4.4)	3.5 ± 3.1 (2.3–7.7)	3.3 ± 3.0 (2.3–7.7)
LWC	34.8 ± 32.7 (4.3–172)	10.1 ± 10.0 (0.2–45.4)	24 ± 30 (0.2–172)
$SNA/PM_{2.5}$ (%)	39.9 ± 6.5 (28.7–54.3)	46.9 ± 8.2 (27.6–60.3)	43.4 ± 8.1 (27.6–60.3)
N/S[b]	1.5 ± 0.3 (0.9–2.4)	1.1 ± 0.2 (0.7–1.5)	1.3 ± 0.4 (0.7–2.4)

[a]Total concentration of SO_4^{2-}, NO_3^-, and NH_4^+.
[b]The ratio of NO_3^-/SO_4^{2-}.

690 **Table 2. Concentrations (ng m^{-3}) of dicarboxylic acids, oxocarboxylic acids, and α-dicarbonyls in PM$_{2.5}$ before and during the LCD in Jinan.**

Compounds	Before the LCD ($n = 36$)	During the LCD ($n = 36$)	Whole period ($n = 72$)
I. Dicarboxylic acids			
Oxalic, C_2	181 ±47.5 (110–381)	239 ±108 (46.0–478)	210 ±87.8 (46.0–478)
Malonic, C_3	14.5 ±4.3 (5.2–26.1)	44.9 ±14.3 (17.8–78.6)	29.7 ±18.5 (5.2–78.6)
Succinic, C_4	53.9 ±28.6 (14.9–178)	30.0 ±12.7 (11.3–66.3)	42.0 ±25.1 (11.3–178)
Glutaric, C_5	6.7 ±4.5 (0.6–19.5)	7.5 ±4.0 (0.7–15.2)	7.1 ±4.2 (0.6–19.5)
Adipic, C_6	9.2 ±8.6 (1.7–40.9)	6.1 ±3.3 (0.9–14)	7.6 ±6.7 (0.9–40.9)
Pimelic, C_7	2.3 ±1.5 (0.2–7.4)	1.9 ±1.4 (0–5.1)	2.1 ±1.5 (0–7.4)
Suberic, C_8	7.7 ±4.7 (1.9–23.0)	3.0 ±2.4 (0.1–13.3)	5.4 ±4.4 (0.1–22.5)
Azelaic, C_9	12.0 ±4.0 (5.8–24.4)	5.9 ±4.8 (0.4–23.1)	9.0 ±5.3 (0.4–24.4)
Sebacic, C_{10}	3.9 ±2.3 (1.3–9.9)	2.6 ±1.5 (0.2– 5.1)	3.3 ±2.0 (0.2– 9.9)
Undecanedioic, C_{11}	4.0 ±2.9 (0.5–15.3)	3.5 ±1.9 (0.3–8.6)	3.8 ±2.4 (0.3–15.3)
Methylmalonic, iC_4	3.5 ±4.1 (0.2–13.1)	4.8 ±4.6 (0–16.9)	4.1 ±4.4 (0–16.9)
Mehtylsuccinic, iC_5	4.2 ±3.5 (0.4–11.7)	3.4 ±1.6 (0.4–6.1)	3.8 ±2.7 (0.4–11.7)
Methyglutaric, iC_6	2.2 ±1.1 (0.4–5.6)	2.4 ±1.4 (0–6.6)	2.3 ±1.3 (0–6.6)
Maleic, M	6.9 ±6.2 (0.8–33.9)	5.0 ±2.3 (0.6–11.0)	5.9 ±4.7 (0.6–34)
Fumaric, F	10.1 ±7.6 (2.3–43.7)	1.5 ±0.9 (0.2–4.8)	5.8 ±6.9 (0.2–43.7)
Methylmaleic, mM	5.5 ±4.3 (1.4–22.4)	4.2 ±3.3 (0–15.7)	4.9 ±3.9 (0–22.4)
Phthalic, Ph	11.0 ±6.1 (2.9–34.4)	8.8 ±6.1 (1.2–25.0)	9.9 ±6.2 (1.2–34.4)
Isophthalic, iPh	3.0 ±3.9 (0.2–23.9)	1.8 ±2.4 (0–9.9)	2.4 ±3.3 (0–23.9)
Terephthalic, tPh	2.0 ±1.4 (0.2–7.5)	1.3 ±0.8 (0.1–2.6)	1.6 ±1.2 (0.1–7.5)
Ketomalonic, kC_3	2.1 ±1.4 (0.3–6.3)	3.0 ±1.7 (0.2–7.4)	2.6 ±1.6 (0.2–7.4)
Ketopimelic, kC_7	5.1 ±4.7 (0.8–20.1)	5.7 ±4.2 (0.2–17.0)	5.4 ±4.4 (0.2–20.1)
Subtotal	351 ±92.2 (212–672)	386 ±127 (121–707)	369 ±112 (121–707)
II. Oxocarboxylic acids			
Pyruvic, Pyr	13.2 ±4.9 (4.4–25.1)	21.3 ±8.8 (7.3–42.6)	17.3 ±8.2 (4.4–42.6)
Glyoxylic, ωC_2	24.1 ±9.1 (6.6–43.0)	28.8 ±8.5 (10.4–43.4)	26.0 ±9.0 (6.6–43.4)
3-Oxopropanoic, ωC_3	4.5 ±4.6 (0.8–24.9)	12.3 ±6.5 (0.6–26.6)	8.4 ±6.9 (0.6–26.6)
4-Oxobutanoic, ωC_4	7.1 ±6.4 (0.8–38.4)	3.1 ±2.7 (0–12.4)	5.1 ±5.3 (0–38.4)
7-Oxoheptanoic, ωC_7	2.3 ±2.2 (0.2–8.6)	1.9 ±2.0 (0–8.6)	2.1 ±2.1 (0–8.6)
8-Oxooctanoic, ωC_8	3.2 ±2.8 (0.4–15.7)	3.7 ±2.1 (0.1–9.3)	3.4 ±2.4 (0.1–15.7)
9-Oxononanoic, ωC_9	6.9 ±3.0 (1.5–14.7)	3.4 ±2.9 (0–9.0)	5.2 ±3.4 (0–14.7)
Subtotal	61.3 ±19.6 (24.6–106)	74.6 ±17.0 (37.0–104)	67.9 ±19.4 (25–106)
III. α-Dicarbonyls			
Glyoxal, Gly	12.6 ±6.3 (4.4–31.8)	13.0 ±5.3 (2.0–28.1)	12.8 ±5.8 (2.0–31.8)
Methyglyoxal, mGly	12.0 ±7.6 (2.6–30.0)	11.7 ±4.8 (2.4–20.9)	11.8 ±6.0 (2.4–29.7)
Subtotal	25.1 ±14.0 (7.8–62.0)	24.7 ±10.0 (4.4–49.0)	24.5 ±11.5 (4.4–61.5)
Total detected species	437 ±117 (246–833)	486 ±144 (179–825)	461 ±132 (179–833)

Table 3. Differences in the stable carbon isotopic compositions ($\delta^{13}C$, ‰) of major detected diacids and related compounds before and during the LCD.

Compounds	Before the LCD ($n = 36$)	During the LCD ($n = 36$)	Whole period ($n = 72$)
I. Dicarboxylic acids			
C_2	−21.6 ± 1.9 (−26.3 to −17.0)	−19.0 ± 2.5 (−23.9 to −14.0)	−20.3 ± 2.5 (−26.3 to −14.0)
C_3	−25.3 ± 4.2 (−36.0 to −19.0)	−22.3 ± 2.2 (−25.6 to −17.9)	−23.8 ± 3.6 (−36.0 to −17.9)
C_4	−27.7 ± 4.6 (−38.8 to −21.6)	−24.6 ± 2.4 (−28.8 to −20.3)	−26.1 ± 4.0 (−38.8 to −20.3)
C_6	−29.0 ± 3.4 (−38.3 to −23.1)	−26.6 ± 2.8 (−31.3 to −21.7)	−27.8 ± 3.3 (−38.3 to −21.7)
C_9	−27.3 ± 1.2 (−29.8 to −25.2)	−27.1 ± 2.3 (−32.3 to −23.9)	−27.2 ± 1.8 (−32.3 to −23.9)
Ph	−38.6 ± 6.4 (−51.1 to −26.6)	−30.2 ± 2.6 (−36.0 to −26.0)	−34.4 ± 6.4 (−51.1 to −26.0)
tPh	−36.5 ± 4.1 (−46.3 to −25.8)	−34.3 ± 0.9 (−35.8 to −31.9)	−35.4 ± 3.1 (−46.3 to −25.8)
II. Oxocarboxylic acids			
Pyr	−28.2 ± 4.0 (−39.0 to −22.3)	−24.0 ± 2.3 (−28.5 to −20.1)	−26.1 ± 3.9 (−39.0 to −20.1)
ωC_2	−26.8 ± 3.6 (−38.4 to −22.4)	−22.7 ± 2.2 (−26.3 to −18.6)	−24.8 ± 3.6 (−38.4 to −18.6)
ωC_3	−29.4 ± 4.0 (−39.8 to −23.7)	−25.9 ± 2.3 (−29.9 to −22.0)	−27.6 ± 3.7 (−39.8 to −22.0)
III. α-Dicarbonyls			
Gly	−23.2 ± 3.7 (−35.6 to −18.5)	−19.6 ± 2.2 (−23.9 to −15.9)	−21.4 ± 3.5 (−35.6 to −15.9)
mGly	−25.3 ± 3.8 (−37.1 to −20.9)	−21.3 ± 2.0 (−24.6 to −17.8)	−23.3 ± 3.6 (−37.1 to −17.8)
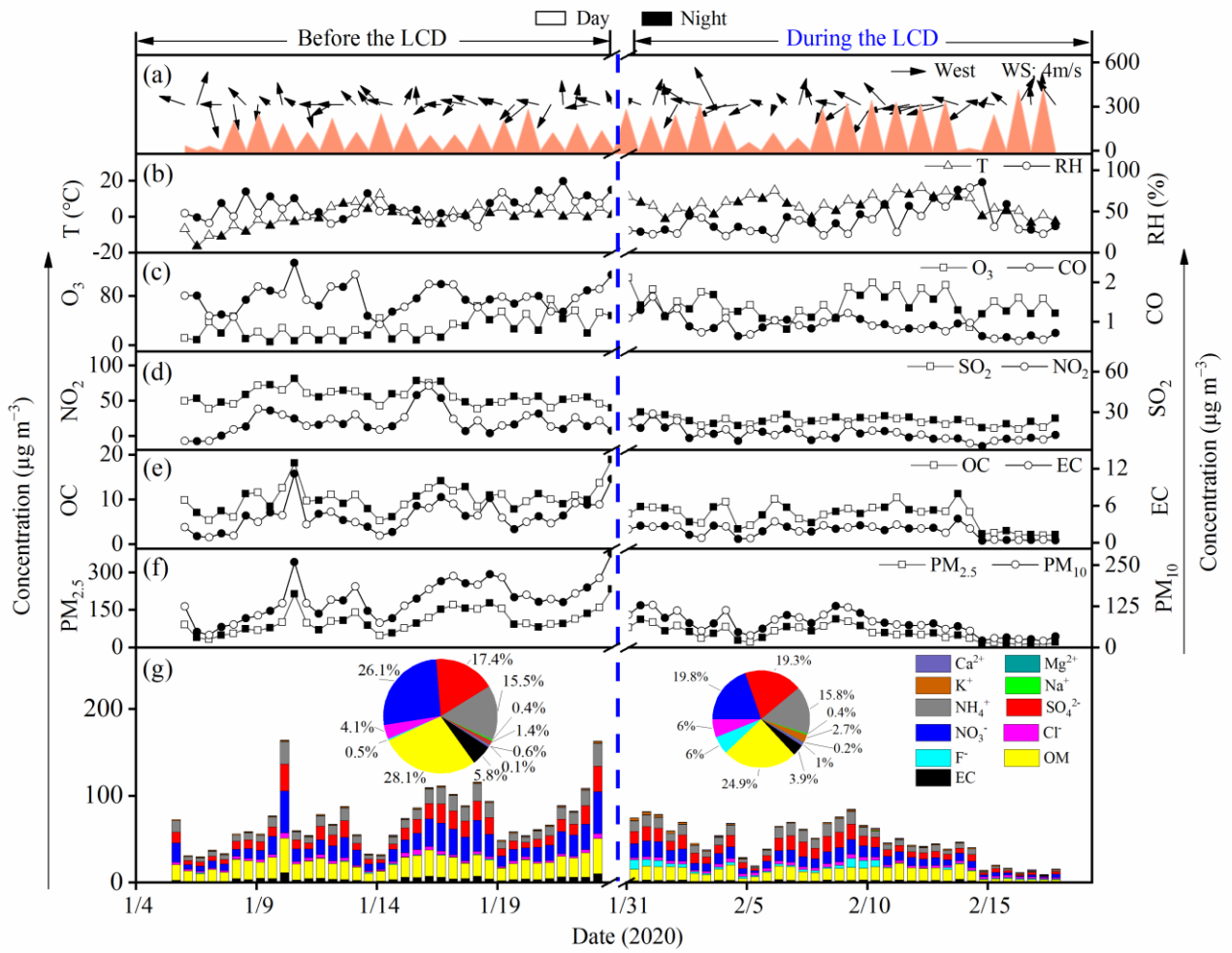
Figure 1. Temporal variations of gaseous pollutants, meteorological parameters, and chemical compositions of PM$_{2.5}$ before and during the LCD.

700
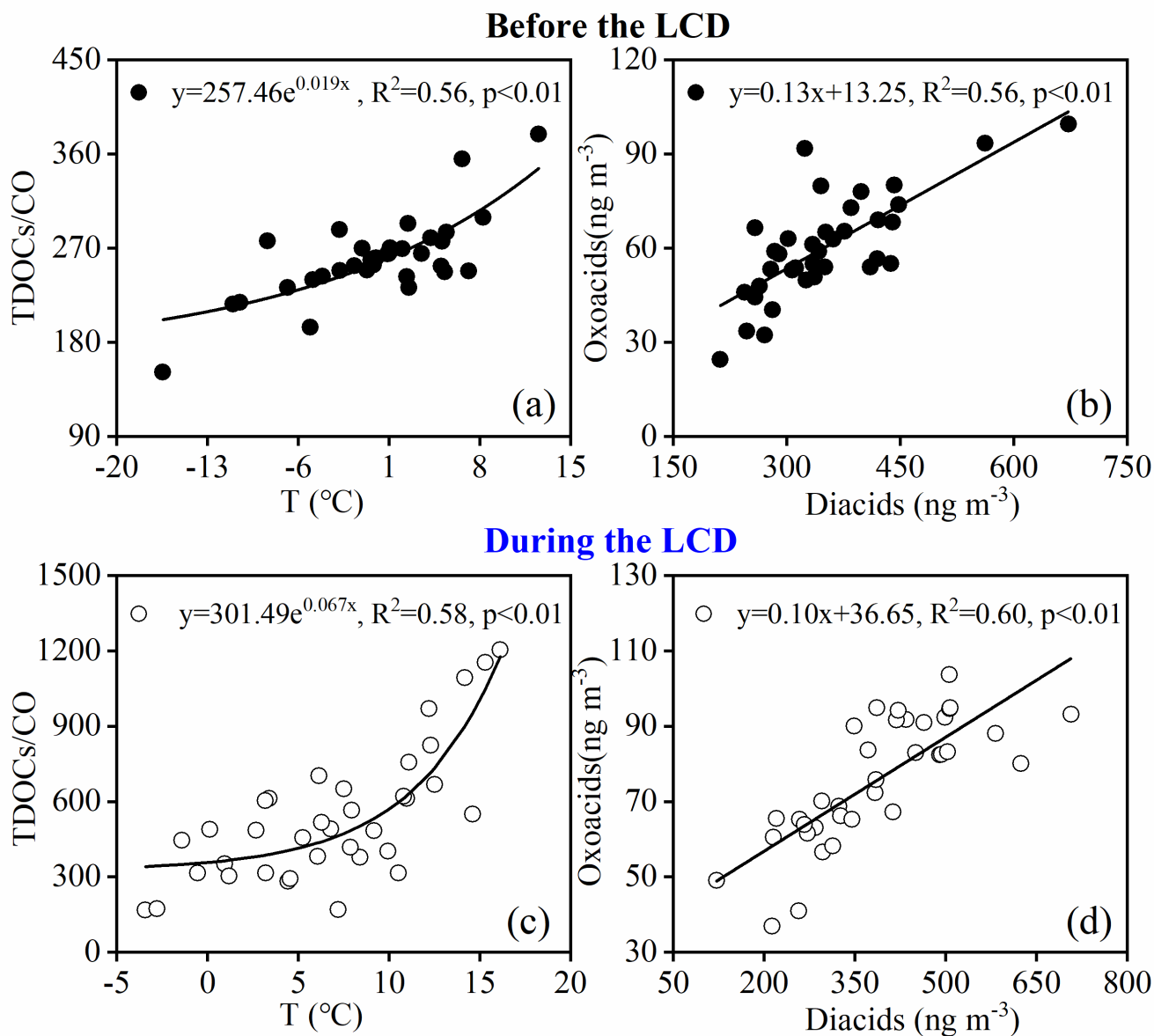
Figure 2. Correlation analysis between concentrations of total detected organic components (TDOCs) and temperature, and between diacids and oxoacids (a) and (b) before the LCD, (c) and (d) during the LCD.
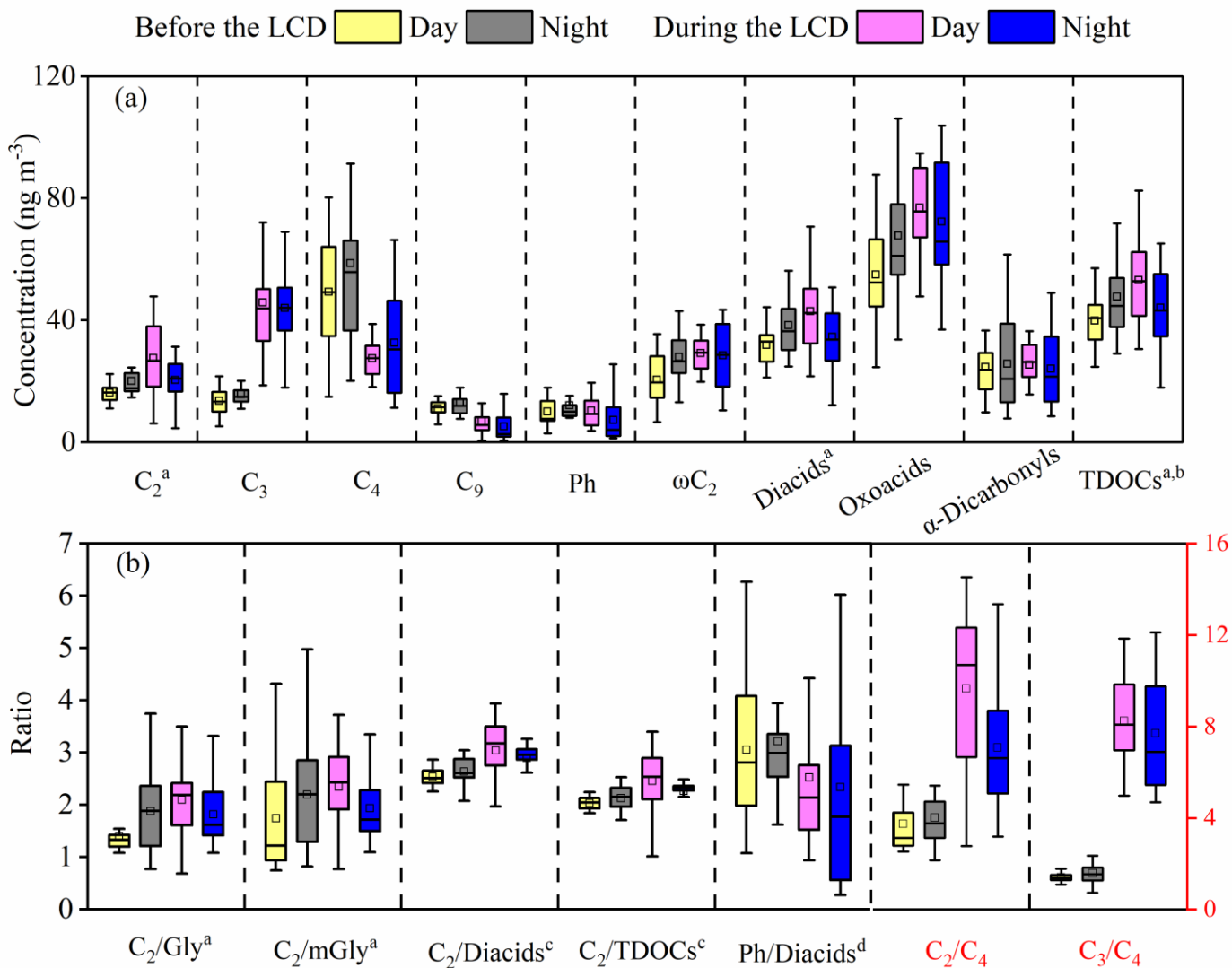
Figure 3. Diurnal changes of (a) major organic compounds and (b) selected mass ratios before and during the LCD ([a] the concentrations reduced by 10 times; [b] TDOCs: total detected organic components; [c] the mass ratios enlarged by 5 times; [d] the mass ratio enlarged by 100 times).
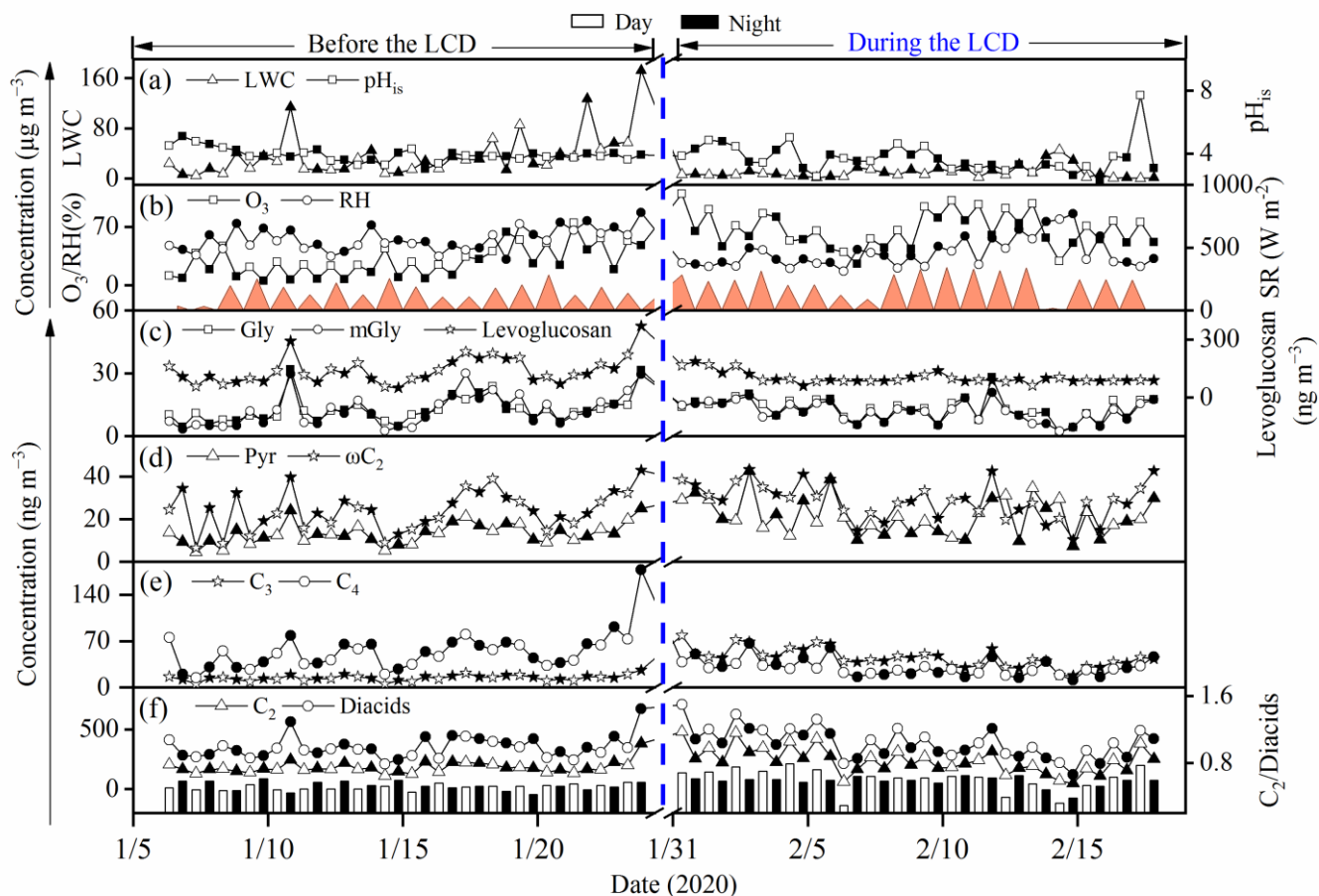
Figure 4. Temporal variations in the concentrations of levoglucosan, diacids, C₂ and its major precursors, the ratios of C₂/Diacids, as well as liquid water content (LWC), in-situ pH (pH$_{is}$), temperature, relative humidity (RH), solar radiation, and O₃ before and during the LCD.
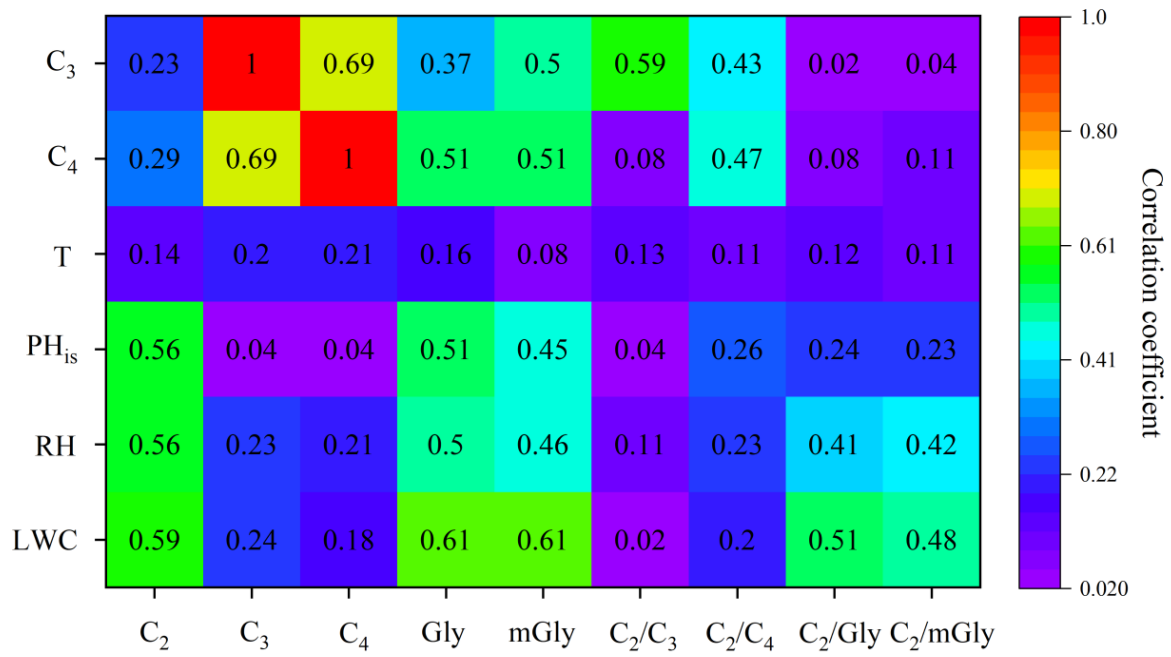
Figure 5. Correlation coefficients (R^2) of concentrations of C_2 and its organic precursors and selected ratios with influencing factors before the LCD.
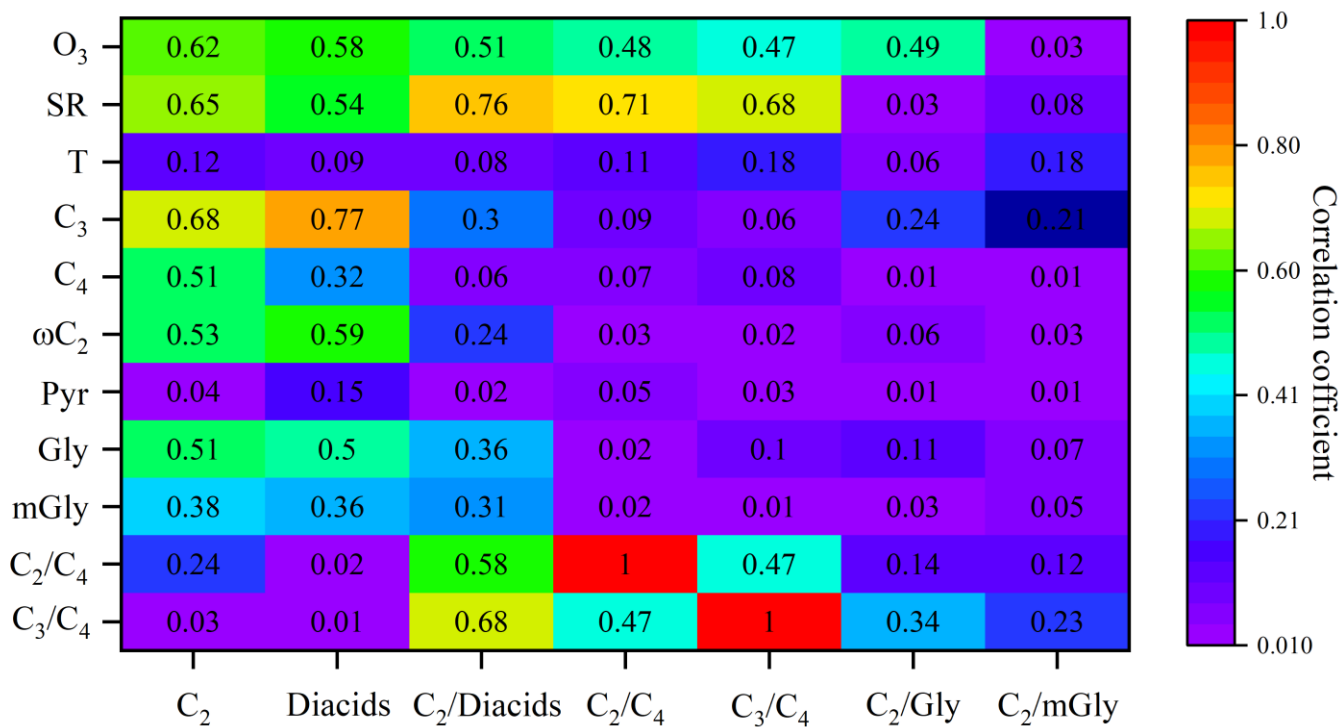
Figure 6. Correlation coefficients (R^2) of concentrations of C_2 and its organic precursors and selected ratios with influencing factors during the LCD.
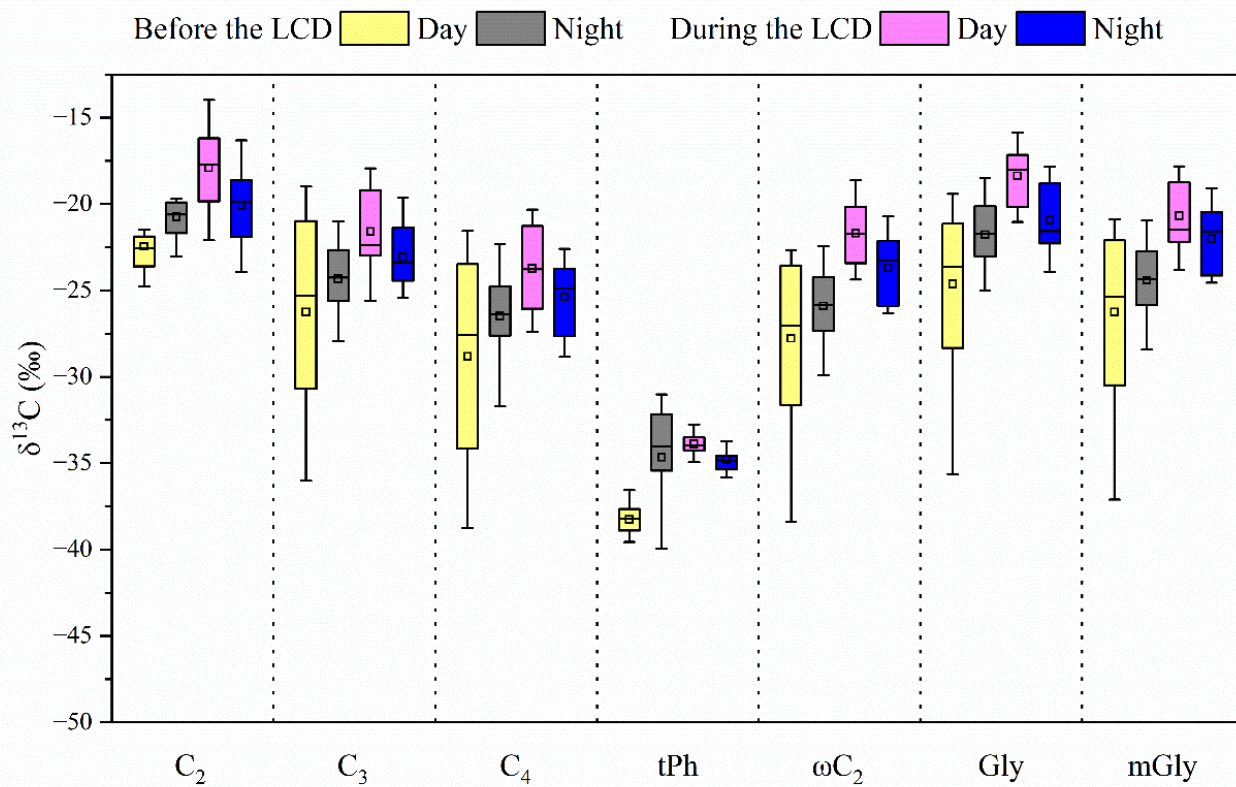
Figure 7. Differences in the stable carbon isotope compositions of major detected diacids (C_2–C_4, tPh), the smallest oxoacids (ωC_2), and α-dicarbonyls including Gly and mGly before and during the LCD in the atmosphere of Jinan.

725
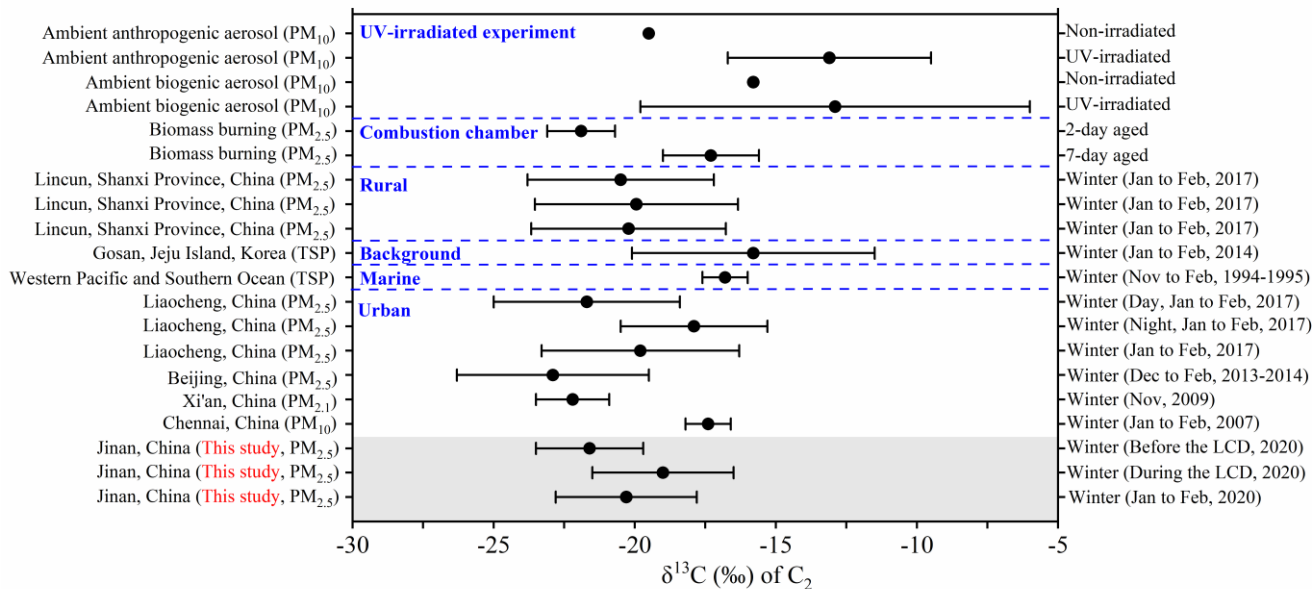
Figure 8. Comparison of stable carbon isotopic compositions (δ¹³C, ‰) of C₂ in aerosols of Jinan with those in other regions in the winter.

Figure 9. Correlations of the $\delta^{13}C$ of C_2 with the mass ratios of C_2/Gly, $C_2/mGly$, $C_2/Diacids$, $C_2/\omega C_2$, and C_2/kC_3, and the $\delta^{13}C$ of tPh with the mass ratio of tPh/Diacids before and during the LCD in January to February 2020.
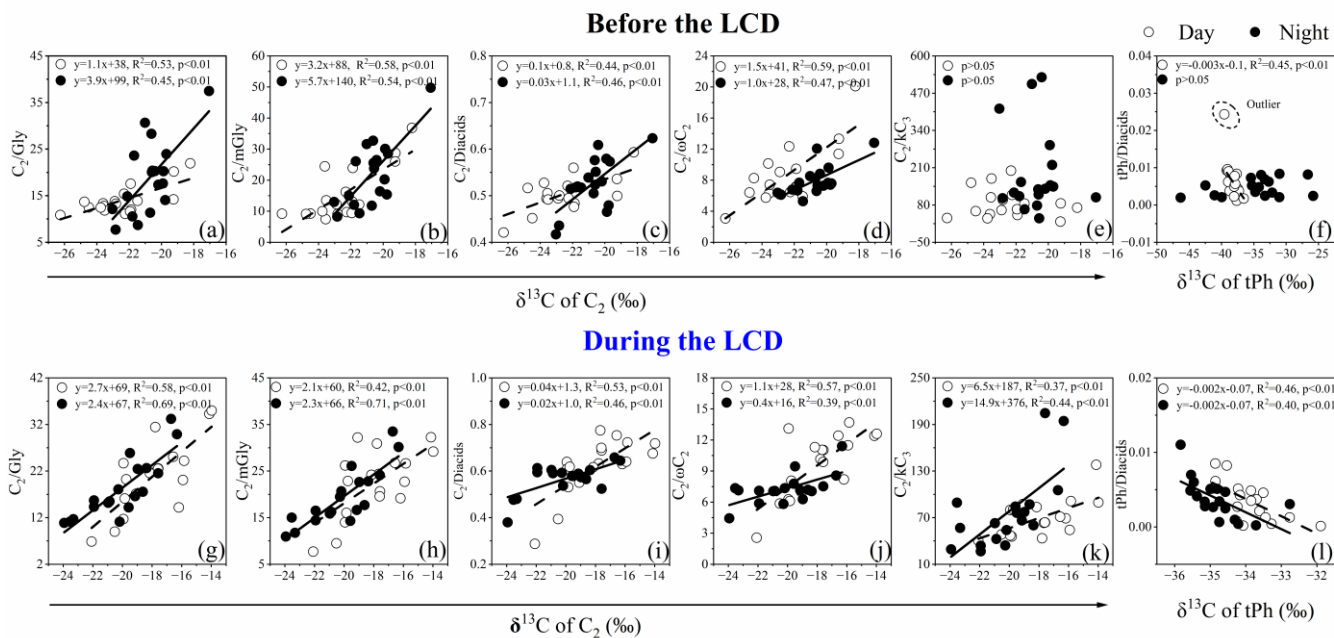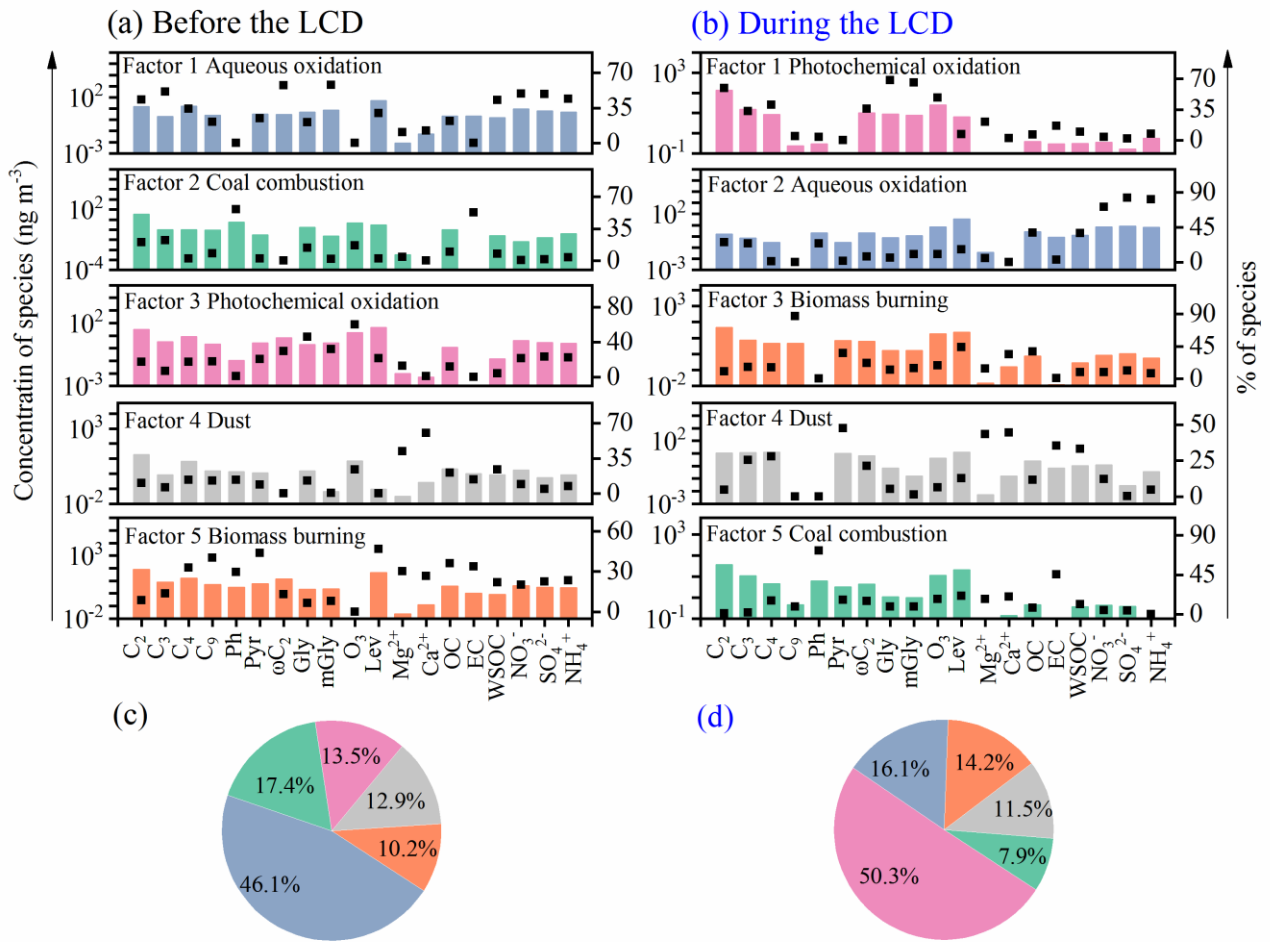
Figure 10. Source profiles of major chemical components in the $PM_{2.5}$ samples from Jinan (a, c) before the LCD and (b, d) during the LCD (BB: biomass burning).